Symmetric Collinear Four-Body Problem via Symbolic Dynamics

Masayoshi Sekiguchi

Doctor of Science

Department of Astronomical Science
School of Mathematical and Physical Science
The Graduate University for Advanced Studies

2001

ADDRESS:

Kisarazu National College of Technology,
Kiyomidai-Higashi 2-11-1, Kisarazu,
Chiba 292-0041, JAPAN

TEMPORARY ADDRESS (Nov.2001-Aug.2002):

Departament de Matemàtica Aplicada i Anàlisi,
Universitat de Barcelona,
Gran Via de les Corts Catalanes, 585
08071 Barcelona, SPAIN

E-MAIL ADDRESS:

masa@yana.kisarazu.ac.jp

Acknowledgments

I would like to express my best appreciation to Professor K. Tanikawa in National Astronomical Observatory Japan for his exact advice, successive encouragement, and comprehensive support over 10 years. He led me to this beautiful and amazing world of Dynamical Systems, especially of Newtonian few-body problem. He constantly gave me chance to discuss on many topics, permitted me to use his office, and helped my research. Without his support, I would have never complete this thesis. I express my thanks to Professors H. Kinoshita, H.Yoshida and M.Yoshikawa for many comments, discussions and continuous encouragements. I am also grateful to Professor W. Sweatman for our valuable discussions on our common topic: symmetric collinear four-body problem. I was greatly encouraged by him and his excellent works.

I would like to express my gratitude to all colleagues at Kisarazu National College of Technology for their many helps and constant encouragements, especially for rich advice of Professors S. Ohuchi and Y. Kashiwagi, for great supports of Professors M. Kamishita, S. Takato and M. Kamata, and for thoughtful encouragements of our students.

Finally, I would like to acknowledge my family who has encouraged and supported me throughout my research and life.

Abstract

Symmetric collinear four-body problem (SC4BP for short) is a special case of the general Newtonian four-body problem in which the bodies are distributed symmetrically about the center of masses on a fixed common line. This is a Hamiltonian system of two degrees of freedom. We analytically study SC4BP independently of the values of mass and energy, and numerically study the case of equal-mass and negative energy. The present work is the first systematic study of SC4BP with the aid of combination of symbolic dynamics, the McGehee's method, and surface of section. It provides rich qualitative features in SC4BP.

Our purpose is to clarify qualitatively the structure of phase space for SC4BP. Almost all orbits for SC4BP experience an infinity of binary collisions. Orbits are replaced by symbol sequences if collisions are replaced by symbols. This replacement enabels us to ignore quantitatively small differences among orbits, but it keeps their qualitative differences. We define a surface of section Σ as the set of central configurations. We can observe all orbits for SC4BP on Σ. Therefore, the study of the phase space is reduced to examine the distribution of symbol sequences on Σ both analytically and numerically.

We express Σ in the phase space described by McGehee's coordinates. As a result, it becomes possible to connect the structure of Σ with the flow on the total collision manifold. We analytically obtain that the set of points leading to quadruple collision forms arcs, which we call *QCC*. Any arc of QCCs forms boundary between regions of different symbol sequences. In addition, we analytically obtain escape criteria by simple two-body consideration. By numerical calculations, we have a distribution of words on Σ. The results show that the distribution of words has the stratified structure in the sea of chaos on Σ divided by some bunches of QCCs. Using the time-reversibility of this autonomous system, one can see that certain subsets of symbol sequences are not realized, and that certain words are possible as periodic orbits. These are closely related to the winding number of the invariant manifolds associated with the critical points on the total collision manifold.

Contents

Chapter 1

Introduction

The symmetric collinear four-body problem (hereafter, referred to as *SC4BP*) is one of special problems for the general four-body system. In SC4BP, four masses $m_4(=m_2)$, $m_3(=m_1)$, m_1, m_2 are put in this order collinearly with their coordinates $q_4(=-q_2)$, $q_3(=-q_1)$, q_1, q_2 and velocities $\dot{q}_4(=-\dot{q}_2)$, $\dot{q}_3(=-\dot{q}_1)$, $\dot{q}_1$, $\dot{q}_2$, respectively. Therefore, SC4BP is a Hamiltonian system with two degrees of freedom. Their initial conditions are given so as to keep the motion symmetric with respect to the origin and collinear for all time. Configuration of SC4BP is shown in Fig.1.1.

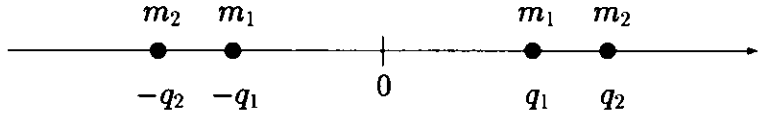

FIG.1.1: Configuration of SC4BP

Though SC4BP is a simple dynamical system, the behavior is complicated, sometimes chaotic. Over the past few decades, a considerable number of studies have been conducted on such a simple dynamical systems, for instance, the collinear three-body problem (hereafter, referred to as *C3BP*), the isosceles three-body problem, or some special four-body problems, and so on. Here we review of a brief history of studies on simple special N-body systems.

1.1 Studies on some special N-body systems

McGehee[21] described C3BP by introducing a set of new *McGehee's variables.* McGehee blew up the total collision singularity to a 2-dimensionl manifold which is pasted on the phase space as a boundary. The manifold is called the *total collision manifold.* McGehee gave a simple proof for one of Sundman's theorems that states impossibility of triple collision in the case of non-zero angular momentum, and un-regularizability of triple collision in general. Since McGehee, a lot of studies on special N-body systems appeared, which are C3BP (Meyer et al[24], Mikkola et al[27, 28, 29],Hietarinta et al[10], Simó[46]Tanikawa et al[56, 57]), the collinear four-body problem (Mather et al[20], Saari et al[39], Tanikawa et al[58]), the isosceles three-body problem (Devaney[3], Moeckel[31],Simó[49], Zare et al[65], and others), the circular-planar restricted three-body problem (Llibre et al[18, 17]), the rectangular case and SC4BP (Simó et al[47]), the trapezoidal four-body problem (Lacomba[12]), the rhomboidal four-body problem (Lacomba[14, 15]), the tetrahedral case (Vidal[59]), the special five-body problem (Xia[63]), etc.

Some of them proved the existence of some special solutions with the aid of *Symbolic Dynamics* which is the basic tool in the studies on N-body systems. Before McGehee, the existence of oscillatory solutions was proved by Sitnikov[51] in spatial restricted three-body problem by using symbolic dynamics. McGehee's tequenic simlified such a proof. Using McGehee's tequenic, Saari and Xia[39] proved the existence of oscillatory solutions in C3BP. In addition, the existence of super-hyperbolic motions was proved for the collinear four-body problem. Mather and McGehee[20] gave a proof of the existence of solutions which become unbounded in finite time for the collinear four-body problem. In their proof, triple collision works effectively in the process of unbounded motion. It is remarkable that Xia[63] proved the existence of non-collision singularity in 5-body systems. Also in their works, triple collision works effectively. The importance of local analyses around the total collision has been recognized through these studies.

These studies wre based on understandings of geometry around the total collision.

On the other hand, studies on the geometry itself were conducted extensively ([3, 12, 14, 15, 17, 46, 47, 59]). As a natural subsequence after the proposition that insists on un-regularizability of triple collision in general, Simó[46] studied masses which enable regularization of triple collision by examininig the connection of invariant manifolds on the total manifold. There are devoted many studies to analyze the local phase structure around the total collision in each special settings. McGehee's tequenic is suitable for such studies because fictitious flow on the total collision manifold reflects real flow near the total collision.

The first study on SC4BP was made by Simó and Lacomba [47]. They concentrated on flow on the total collision manifold, especially, on the invariant manifolds associated with the critical points. They determined some values of mass ratio where the invariant manifolds change their behavior qualitatively, as well as behavior near the total collision chages qualitatively. Althogh McGehee's technique enables to study the local structure, it can not give any information on global behaviors in dynamical systems. For comprehension of global behaviors of solutions, the method of *Surface of Section* is used well. It bases on numerical analyses in most cases. Mikkola et al[27, 28, 29] conducted an extensive numerical simulations for the collinear three-body problem and examined the structure in the surface of section. As a result, they clarified the global phase structure. Similarly, Sweatman[55] carried out a numerous number of numerical simulations for SC4BP and observed their orbits on the surface of section. They obtained some interesting orbits, and divided them into three categories according to their qualitative behaviors, which are *quasiperiodic, fast-scattering* and *chaotic* motions. They pointed out similarity of the surface of section in SC4BP to one in collinear three-body problem. They insisted that SC4BP is the simplest model for collisions of two pairs of binaries. Although some generalization is required to study such a process of binary-binary collision, it is basically neccesary to clarify the process in the simplest model. However, both of them did not pay attension to any influence from the total collision to the global phase structure.

On the contrary, Tanikawa et al[56, 57] noticed importance of the total collision

when they applied symbolic dynamics to the collinear three-body problem. They obtained that a set of initial points to the total collision slices *chaotic area* which were already discovered by Mikkola et al[27, 28, 29]. However, their study was mainly based on numerical simulations, and contained no strict proof on the stratified structure becuaue it did not share in the bounty of the total collision analyses. Tanikawa et al[58] carried out a huge number of numerical simulations of the free-fall colllinear four-body problem. They obtained a complicated and interesting structure in the initial value space, which seemed to form fractals. In this case, it is expected to find a special solution which becomes unbounded within a finite time. Zare et al[65] applied symbolic dynamics to the isosceles three-body problem, clarified structure of phase space in the system. They found structure in the chaotic regions as well. Symbolic dynamics work effectively for study of a certain class of dynamical systems like these.

1.2 Outline of the present paper

In these previous studies, several analytical tools or extensive numerical simulations are used independently. In the present paper, we combine two methods of symbolic dynamics and surface of section with the aid of McGehee's variables. We intend to analyze the structure of distribution of symbol sequences on the surface of section, analytically and numerically. Gooal of the present paper is to comprehend the whole structure of phase space in SC4BP.

In chapter 2, we formulate SC4BP, introduce variables of McGehee and define the total collision manifold. The total collision manifold is important, also in SC4BP. We call it *Quadruple Collision Manifold* (*QCM*, for short). Flows on QCM greatly reflect the global behavior as well as the local behavior of solutions near the quadruple collision. When the total energy is negative, orbits are realized in the interior of QCM. Our surface of section Σ is defined as a section of QCM with its interior. It is possible to understand structure of Σ in combination with flow on QCM. In SC4BP, almost all the solutions experience binary collisions. We make a correspondence

from solutions to a sequence of binary collisions which are denoted by some symbol sequences. Thus, we can apply symbolic dynamics to SC4BP. We associate to any point on a surface of section a symbol sequence.

In chapter 3, we describe our analytical results. Flows on the QCM and the homothetic solution are given. The surface of section Σ is proved to be global, i.e., arbitrary orbits of SC4BP have an intersection with Σ at least. Reversibility of Σ is confirmed. Immediate future of solution crossing Σ is predicted. The set of points on Σ leading to quadruple collision is discussed. They form one dimensional curves on Σ which we call *Quadruple Collision Curves* (QCC, for short). Finally, we obtain the escape criteria by two-body consideration.

In chapter 4, results of numerical calculations are described. The surface of section is sliced by QCCs into an infinity of stratified areas. We divide Σ into 12 regions based on the main QCCs. We find some un-realizable sequences of symbols from numerical calculations directly. We assume one property which is confirmed by numerical calculations partially. We construct all unrealizable sequences from the property, which we propose as a conjecture. Studying spatial order of QCCs yeilds the clear understanding of fractal structure in the area where are an infinity of QCCs. We find a transition rule among another set of 12 regions. This enables us to construct some possible periods of periodic points of Σ. Other calculations display families of periodic points, invariant regions, and escape regions on Σ.

Chapter 2

Methods

Main purposes in this chapter are to define a surface of section, to define the correspondence between orbits and symbol sequences, and to give some terminologies, which are used both analytically and numerically. First, we describe equations of motion and their singularities. Second, we give a transformation of variables in order to remove singularities due to collisions. We blow up singularity due to quadruple collision. Blow-up technique enables us to analyze the behavior of orbits in the vicinity of quadruple collision. We regularize binary collisions. Regularization enables us to continue orbits beyond binary collision. New variables are applicable to analytical studies as well as numerical integrations. We embed the phase space into the 3-dimensional space using the new variables. Third, we define a surface of section. Also, we give a coordinate system to the surface of section by the new variables. Finally, we define an assignment of symbols to physical events as well as replacement of orbits by symbol sequences. This simplification enables us to neglect quantitatively small differences among orbits and to concentrate their qualitative differences.

2.1 Equations of Motion

From formulation of SC4BP (see Fig.1.1) the Lagrangian function is obtained as below.

$$L = \frac{1}{2}\,{}^t\dot{\boldsymbol{q}} M \dot{\boldsymbol{q}} + U(\boldsymbol{q}),$$

where $\boldsymbol{q} = {}^t(q_1, q_2)$, $M = \mathrm{diag}(2m_1, 2m_2)$ and the force function

$$U(\boldsymbol{q}) = \frac{m_1^2}{2q_1} + \frac{m_2^2}{2q_2} + \frac{2m_1m_2}{q_1+q_2} + \frac{2m_1m_2}{q_2-q_1}.$$

Here we assume the gravitation constant to be unity($G = 1$). Momentum $\boldsymbol{p} = {}^t(p_1, p_2)$ conjugate to $\boldsymbol{q}$ is defined by

$$p_i = \frac{\partial L}{\partial \dot{q}_i} = 2m_i\dot{q}_i, \qquad (i = 1, 2).$$

Then we have Hamiltonian equations of motion, i.e.

$$\dot{q}_i = \frac{\partial H}{\partial p_i}, \qquad \dot{p}_i = -\frac{\partial H}{\partial q_i}, \qquad (i = 1, 2), \tag{2.1.1}$$

with Hamiltonian function

$$H = \frac{1}{2}\,{}^t\boldsymbol{p} M^{-1} \boldsymbol{p} - U(\boldsymbol{q}).$$

This dynamical system is defined in the domain(see Fig.2.1)

$$\{(q_1, p_1, q_2, p_2) \in \Re^4 \mid 0 < q_1 < q_2\}. \tag{2.1.2}$$

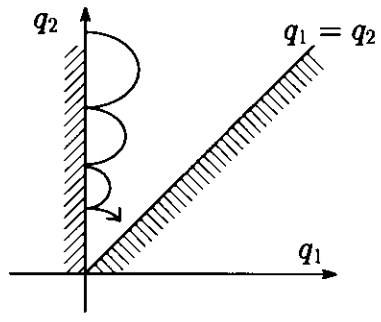

FIG.2.1: Configuration Space for SC4BP

Boundaries($q_1 = 0$, $q_1 = q_2 \neq 0$ and $q_1 = q_2 = 0$) give rise to different singularities in the equations of motion(2.1.1). These singularities are named as *1-2-1 binary*

collision ($q_1 = 0$), *2-2 binary collision* ($q_1 = q_2 \neq 0$) and *quadruple collision* ($q_1 = q_2 = 0$).

The other singularity occurs in the case($q_1 \to \infty$ or $q_2 \to \infty$). This singularity is named as *escape*. Physically, there are three types of escapes: *2-2 escape* ($q_2 \to \infty$ while q_1 is bounded), *1-2-1 escape* ($q_1 \to \infty$ while $|q_2 - q_1|$ is bounded), and *total escape* ($|q_2 - q_1| \to \infty$ as $q_1 \to \infty$). In the case of negative energy, the third case never occurs.

We can assume $m_1 + m_2 = 1$ without loss of generality. We use a new variable φ instead of masses m_1 and m_2, i.e.,

$$\sqrt{m_1} = \cos\varphi, \qquad \sqrt{m_2} = \sin\varphi,$$

where $\varphi \in (0, \frac{\pi}{2})$. Then we have a new expression of the force function $U(\boldsymbol{q})$, i.e.

$$U(\boldsymbol{q}) = \frac{\cos^4\varphi}{2q_1} + \frac{\sin^4\varphi}{2q_2} + \frac{2\sin^2\varphi\cos^2\varphi}{q_1 + q_2} + \frac{2\sin^2\varphi\cos^2\varphi}{q_2 - q_1}.$$

This enables us to describe the elegant expressions of the force function and the domain as seen in the next section.

2.2 Blow-up and Regularization

First, we remove a singularity due to quadruple collision($q_1 = q_2 = 0$) from the equations (2.1.1) by the following transformation: blow-up technique.

$$r = \sqrt{2(q_1^2\cos^2\varphi + q_2^2\sin^2\varphi)}, \tag{2.2.1}$$

$$\cos\theta = \sqrt{2}q_1\cos\varphi/r,$$

$$\sin\theta = \sqrt{2}q_2\sin\varphi/r,$$

$$v = (q_1p_1 + q_2p_2)/\sqrt{r},$$

$$u = (q_1p_2\cot\varphi - q_2p_1\tan\varphi)/\sqrt{r},$$

$$d\tau = r^{-3/2}dt.$$

Thereby, we obtain a new set of equations of motion;

$$\begin{aligned} \frac{dr}{d\tau} &= rv, \\ \frac{d\theta}{d\tau} &= u, \\ \frac{dv}{d\tau} &= \frac{1}{2}v^2 + u^2 - V(\theta), \\ \frac{du}{d\tau} &= -\frac{uv}{2} + \frac{dV(\theta)}{d\theta}, \end{aligned} \tag{2.2.2}$$

where

$$V(\theta) = \frac{1}{\sqrt{2}}\Big(\frac{\cos^5\varphi}{\cos\theta} + \frac{\sin^5\varphi}{\sin\theta} + \frac{\sin^3 2\varphi\cos\varphi\sin\theta}{\sin(\theta+\varphi)\sin(\theta-\varphi)}\Big), \tag{2.2.3}$$

Hamiltonian function is rewritten to the following equation:

$$rh = \frac{1}{2}(v^2 + u^2) - V(\theta), \tag{2.2.4}$$

where h is a value of the total energy.

The domain (2.1.2) is translated to

$$\{(r,\theta,v,u) \in \Re^4 \mid r > 0, \varphi < \theta < \pi/2\}.$$

Boundaries of (2.1.2): $q_1 = q_2 = 0$, $q_1 = q_2 \neq 0$, $q_1 = 0$ are also translated to $r = 0$, $\theta = \varphi$, $\theta = \pi/2$, respectively. One can extend the domain to its boundary $r = 0$ because (2.2.2)-(2.2.4) are still regular if $r = 0$. Therefore, we take a new domain, i.e.,

$$\{(r,\theta,v,u) \in \Re^4 \mid r \geq 0, \varphi < \theta < \pi/2\}. \tag{2.2.5}$$

These variables enable us to describe the flow in the vicinity of the quadruple collision. On the other hand, binary collisions($\theta = \varphi$ and $\theta = \pi/2$) still remain as singularities of the (2.2.2).

Second, we regularize binary collision singularities ($\theta = \varphi$ or $\theta = \pi/2$) by the following transformation.

$$\begin{aligned} W(\theta) &= V(\theta)\cos\theta\sin(\theta-\varphi), \\ w &= \frac{\cos\theta\sin(\theta-\varphi)}{\sqrt{W(\theta)}}u, \end{aligned} \tag{2.2.6}$$

$$ds = \frac{\sqrt{W(\theta)}}{\cos\theta\sin(\theta-\varphi)}d\tau.$$

Thereby, we obtain the equations of motion

$$\frac{dr}{ds} = rv\frac{\cos\theta\sin(\theta-\varphi)}{\sqrt{W(\theta)}}, \tag{2.2.7}$$

$$\frac{d\theta}{ds} = w,$$

$$\frac{dv}{ds} = \sqrt{W(\theta)} + (2hr - \frac{v^2}{2})\frac{\cos\theta\sin(\theta-\varphi)}{\sqrt{W(\theta)}},$$

$$\frac{dw}{ds} = \frac{2\cos\theta\sin(\theta-\varphi) - w^2}{2W(\theta)}\frac{dW(\theta)}{d\theta} - \frac{vw\cos\theta\sin(\theta-\varphi)}{2\sqrt{W(\theta)}}$$

$$+ \cos(2\theta-\varphi)\Big(1 + (2hr - v^2)\frac{\cos\theta\sin(\theta-\varphi)}{W(\theta)}\Big),$$

with the energy relation translated from (2.2.4)

$$(hr - \frac{v^2}{2})\Big(\frac{\cos\theta\sin(\theta-\varphi)}{\sqrt{W(\theta)}}\Big)^2 = \frac{w^2}{2} - \cos\theta\sin(\theta-\varphi). \tag{2.2.8}$$

These are not yet canonical equations. The domain (2.2.5) is translated to

$$\{(r,\theta,v,w) \in \Re^4 \mid r \geq 0, \varphi < \theta < \pi/2\}.$$

One can extend this domain to its boundaries $\theta = \varphi$ and $\theta = \pi/2$ because (2.2.6)-(2.2.8) are still regular if $\theta = \varphi$ and $\theta = \pi/2$. Therefore, we have a new domain $\mathcal{D}$, namely

$$\mathcal{D} \equiv \{(r,\theta,v,w) \in \Re^4 \mid r \geq 0, \varphi \leq \theta \leq \pi/2\}. \tag{2.2.9}$$

Thus, the flow beyond the binary collisions is obtained, and singularities due to collisions are removed.

The domain $\mathcal{D}$ is a 3-dimensional subset embedded in 4-dimensional Euclidean space because the motion is realized on the energy surface defined by (2.2.8). In fact, values of r can be determined from other variables through (2.2.8) if $\varphi < \theta < \pi/2$ and $h \neq 0$. Let $\mathcal{D}'$ denote a subset of $\mathcal{D}$ from which $\theta = \varphi$ and $\theta = \pi/2$ are removed.

We embed $\mathcal{D}'$ into the space (θ, v, w) if $h \neq 0$. If we substitute $h = 0$ to (2.2.8), then we have a relation, i.e.,

$$\frac{v^2}{2}\Big(\frac{\cos\theta\sin(\theta-\varphi)}{\sqrt{W(\theta)}}\Big)^2 + \frac{w^2}{2} = \cos\theta\sin(\theta-\varphi). \tag{2.2.10}$$

The 2-dimensional manifold denoted by (2.2.10)(see Fig.2.2) is named as C_0.

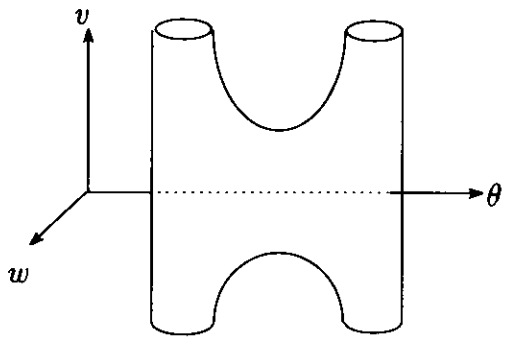

FIG.2.2: Schematic explanation of the phase space for SC4BP

2-dimensional manifold C_0 is homeomorphic to a 2-dimensional sphere with 4 holes.

If $h < 0$ (resp. $h > 0$), the phase space is inside (resp. outside) of C_0. When $h = 0$, the phase space is a direct product of an interval $[0, \infty)$ and C_0. C_0 can be obtained by substituting $r = 0$ into (2.2.8) as well. Therefore, we call C_0 "quadruple collision manifold". Namely,

$$C_0 \equiv \{(r, \theta, v, w) \in \Re^4 \mid r = 0, \varphi \leq \theta \leq \pi/2\}. \tag{2.2.11}$$

2.3 Surface of Section

We define θ_c as the real root of the following equation.

$$\frac{dV(\theta)}{d\theta} = 0.$$

This root θ_c depends on mass parameter φ only (see Appendix A).

Definition 2.3.1 (Surface of Section)

We define a surface of section Σ as follows.

$$\Sigma = \{(r, \theta, v, w) \in \mathcal{D}' \mid \theta = \theta_c\}$$

No solution other than the homothetic solution is tangent to Σ from uniqueness of solution in SC4BP. Moreover, all orbits except for the homothetic solution intersect Σ transversally. The proof is given in the next chapter. Therefore, it is sufficient to study Σ instead of whole set of orbits of SC4BP.

Suppose that there exists an orbit intersecting Σ at least twice. Then we define the mapping on Σ itself.

Definition 2.3.2 (Mapping on Σ)

When an orbit intersecting Σ at $\boldsymbol{x}_0 \in \Sigma$ intersects Σ again at $\boldsymbol{x}_1 \in \Sigma$, mapping $T : \Sigma \to \Sigma$ is defined as

$$T : \boldsymbol{x}_0 \mapsto \boldsymbol{x}_1 = T(\boldsymbol{x}_0)$$

Let us give coordinates to Σ in terms of our new variables. If we substitute $\theta = \theta_c$ into (2.2.8), then we have

$$\frac{v^2}{2} + \frac{W(\theta_c)}{\cos^2\theta_c \sin^2(\theta_c - \varphi)} \frac{w^2}{2} = \frac{W(\theta_c)}{\cos\theta_c \sin(\theta_c - \varphi)} + hr. \tag{2.3.1}$$

Variable r can be uniquely determined from v and w through (2.3.1) if $h \neq 0$. Variables v and w form an ellipse for each values of r if the right-hand side of (2.3.1) is positive. We can take two coordinates v and w on Σ.

In the case of negative energy (e.g. $h = -1$), when range of r is 0 to $W(\theta_c)/\{\cos\theta_c \sin(\theta_c - \varphi)\}$, the right-hand side of (2.3.1) is positive or zero. Thus Σ forms an elliptic disk with its axes $2\sqrt{2V(\theta_c)}$ and $2\sqrt{2\cos\theta_c \sin(\theta_c - \varphi)}$(Fig.2.3). One of axes($w = 0$) of the elliptic disk is the homothetic solution itself. The outermost ellipse is an intersection with C_0(Fig.2.4).

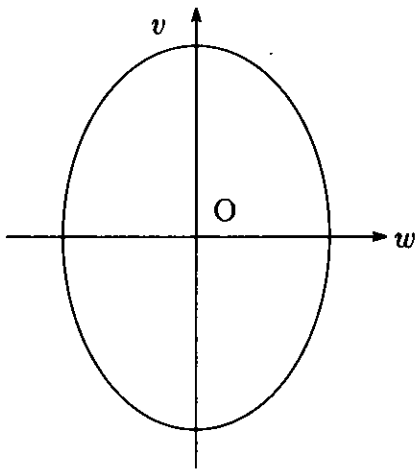

FIG.2.3: Surface of section Σ

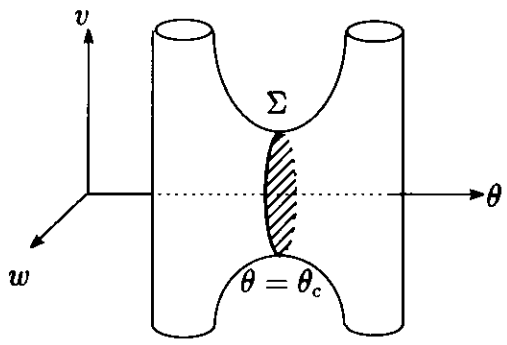

FIG.2.4: Quadruple Collision Manifold C_0 and Surface of section Σ

2.4 Symbol Sequences

We define three symbols given in the following Table 2.1 and dot(.) to denote an intersection of orbit with Σ at the time origin $t = 0$.

symbols(n_i)	values of variables	physical events
0	$\theta = \pi/2$	single binary collision
1	$r = 0$	quadruple collision
2	$\theta = \varphi$	simultaneous binary collision

Table 2.1: Assignment of Symbols

A symbol sequence is constructed in such a way that when a certain physical event listed in Table 2.1 occurs, the corresponding symbol is concatenated rightward. In general, it is impossible to continue orbits beyond quadruple collision. So, we regard as 1 continuing endlessly after the first 1 in the future and before the last 1 in the past, if 1 appears in the sequence.

Now, let us express an orbit passing through $\boldsymbol{x}_0 \in \Sigma$ at $t = 0$ as a sequence of 0, 1 and 2 as follows:

$$[\cdots n_{-2}n_{-1}.n_0n_1n_2\cdots],$$

where $n_k, (k \in \boldsymbol{Z})$ are either 0, 1, or 2. We follow the orbit starting from $\boldsymbol{x}_0 \in \Sigma$ at $t = 0$ to the future and to the past. Then, n_0 represents the first collision. Symbols

n_1, $n_2, \cdots$ represent the second and the latter collisions. Similarly, n_{-1}, $n_{-2}, \cdots$ represent past collisions.

Symbol sequences consist of an infinity of symbols. If we truncate the symbol sequences with finite symbols, then we call them *words*. In the numerical investigations, we often study the distribution of words on Σ.

Thus, we have a definition of the correspondence between a point on Σ and a symbol sequence.

Definition 2.4.1 (Correspondence between Σ and Symbol Sequences)

Let $\phi(\boldsymbol{x}_0)$ denote an orbit passing through $\boldsymbol{x}_0 \in \Sigma$ at $t = 0$, $\Omega(\Sigma)$ denote the set of $\phi(\boldsymbol{x}_0)$, and $\mathcal{B}$ denote the set of all bi-infinite sequences $[\cdots n_{-2}n_{-1}.n_0n_1n_2\cdots]$ of three symbols. Then, we can define the mapping $\mathcal{S} : \Omega(\Sigma) \to \mathcal{B}$ as $\mathcal{S} : \phi(\boldsymbol{x}_0) \mapsto [\cdots n_{-2}n_{-1}.n_0n_1n_2\cdots]$. Simply, we regard $\mathcal{S}$ as a mapping $\Sigma \to \mathcal{B}$, i.e.,

$$\mathcal{S}(\boldsymbol{x}_0) = [\cdots n_{-2}n_{-1}.n_0n_1n_2\cdots]$$

Let X be a subset of Σ. We have an extension of $\mathcal{S}$ as $X \to \mathcal{B}$. In other word, when any point in a certain region $X \subset \Sigma$ has the same symbol sequence $\mathcal{S}_0$, we have the other notations $\mathcal{S}(X) = \mathcal{S}_0$, or $X = \mathcal{S}^{-1}(\mathcal{S}_0)$.

The correspondence between Σ and words is defined similarly.

The following mapping is usually used for discussion in dynamical system. We also introduce it here.

Definition 2.4.2 (Shift map on $\mathcal{B}$)

The shift operator σ is defined by

$$\sigma[\cdots n_{-2}n_{-1}.n_0n_1n_2\cdots] = [\cdots n_{-2}n_{-1}n_0.n_1n_2\cdots].$$

If an orbit repeats the same binary collisions for $t > 0$, it escapes to infinity, otherwise it experiences the other binary collision. If a symbol sequence has an infinity of 0 rightward, i.e., $[\cdots n_{-1}.n_0n_1\cdots 0^\infty]$, then the orbit goes to 1-2-1 escape, i.e.,

$$\lim_{t\to\infty} r = \infty, \qquad \lim_{t\to\infty} \theta = \frac{\pi}{2}$$

If a symbol sequence has an infinity of 2 rightward, i.e., $[\cdots n_{-1}.n_0 n_1 \cdots 2^\infty]$, then the orbit goes to 2-2 escape, i.e.,

$$\lim_{t\to\infty} r = \infty, \qquad \lim_{t\to\infty} \theta = \varphi$$

Thus, we have expressions of escape in terms of symbolic dynamics.

Lemma 2.4.1 (Necessary Condition for Escape in terms of Symbolic Dynamics)
If a symbol sequence σ ends up with an infinity of symbols 0 or 2, then its corresponded orbit goes to infinity.

We apply this condition in our numerical study.

Chapter 3

Analytical Results

Main purpose in this chapter is to display our analytical results. First, we define the Quadruple Collision Manifold which is one of invariant manifolds under the transformed flow. And we show that the fictitious flow restricted on QCM is gradient-like with respect to v. This property influences the flow near the quadruple collision. We give an analytical expression of the homothetic solution which is uniquely determined for SC4BP. The homothetic solution connects two critical points on QCM. Second, we give a proof that the surface of section Σ is global, and a proof of reversibility of Σ. We prove that Σ can be divided into three subregions: Σ_+, Σ_- and Σ_0 according to collision-types orbits undergo after passing each subregion. In the discussion, we obtain several un-realizable words of symbols. It is shown that points leading to the quadruple collision form one-dimensional curves. We call them *Quadruple Collision Curves* (QCC, for short). QCCs have various geometric features. Finally, we obtain escape criteria by simple two-body considerations. We evaluate them on Σ directly. The results give two regions on Σ where points lead to escape immediately. Escape criteria can be used in numerical calculations. They enable us to save time for calculations when the solution satisfies the criteria on the way of integration. If we summarize our analytical results and apply it to the surface of section Σ, then we can expect some stratified structure of Σ.

3.1 Flow on the Quadruple Collision Manifold

If we substitute $r = 0$ into the first equation of (2.2.7), then we have the following equation.

$$\frac{dr}{ds} = 0. \tag{3.1.1}$$

Therefore, the manifold obtained by substituting $r = 0$ into (2.2.8) is an invariant manifold for SC4BP. This is already obtained as (2.2.10) or C_0(Fig.2.2), i.e.,

$$\frac{v^2}{2}\Big(\frac{\cos\theta\sin(\theta-\varphi)}{\sqrt{W(\theta)}}\Big)^2 + \frac{w^2}{2} = \cos\theta\sin(\theta-\varphi).$$

If we substitute $r = 0$ into the other equations of (2.2.7), then we have the following equations.

$$\begin{aligned}
\frac{d\theta}{ds} &= w, \qquad (3.1.2)\\
\frac{dv}{ds} &= \sqrt{W(\theta)} - \frac{v^2}{2}\frac{\cos\theta\sin(\theta-\varphi)}{\sqrt{W(\theta)}},\\
\frac{dw}{ds} &= \frac{2\cos\theta\sin(\theta-\varphi) - w^2}{2W(\theta)}\frac{dW(\theta)}{d\theta} - \frac{vw\cos\theta\sin(\theta-\varphi)}{2\sqrt{W(\theta)}}\\
&\quad + \cos(2\theta-\varphi)\Big(1 - v^2\frac{\cos\theta\sin(\theta-\varphi)}{W(\theta)}\Big).
\end{aligned}$$

The flow on C_0 defined by these equations is fictitious. This fictitious flow reflects physical flow in the vicinity of quadruple collision. There are some significant features.

There are two critical points on C_0, i.e.,

$$(r,\theta,v,w) = (0,\theta_c,\pm\sqrt{2V(\theta_c)},0)$$

We give a name c^+ for the upper one, and c^- for the lower one(see Fig.3.1). These are saddle points on C_0. Each of them have two pairs of 1-dimensional stable and unstable manifolds on C_0(see Appendix A). They coil themselves around arms or body of C_0(Simó[47]).

In addition, there is another significant feature.

Lemma 3.1.1 : (Gradient-like Flow)

$$\frac{dv}{ds} > 0$$

proof

When the energy relation (2.2.10) is applied to the first equation of (3.1.2),

$$\frac{dv}{ds} = \frac{w^2}{2}\frac{\sqrt{W(\theta)}}{\cos\theta\sin(\theta-\varphi)} > 0,$$

if $\varphi < \theta < \pi/2$. If $\theta = \varphi$ or $\theta = \pi/2$, the equation is evaluated directly, i.e.,

$$\theta = \varphi \Longrightarrow \frac{dv}{ds} = \sqrt{W(\varphi)} = 2^{3/4}\sin^{3/2}\varphi\cos^2\varphi > 0$$

$$\theta = \pi/2 \Longrightarrow \frac{dv}{ds} = \sqrt{W(\pi/2)} = 2^{-1/4}\cos^3\varphi > 0$$

Q.E.D.

3.2 The Homothetic Solution and its Invariant Manifolds

There is the homothetic solution for SC4BP, i.e.,

$$\boldsymbol{h}(s) = (2\kappa^2\mathrm{sech}^2(s\lambda+\alpha), \theta_c, -2\kappa\tanh(s\lambda+\alpha), 0), \tag{3.2.1}$$

where $\lambda = \sqrt{\cos\theta_c\sin(\theta_c-\varphi)/2}$, $\kappa = \sqrt{V(\theta_c)/2}$, and a certain real number α. $\boldsymbol{h}(s)$ connects two critical points on C_0 : c^+ and c^-. It takes an infinitely long time for departing from c^+ and reaching c^-(see Appendix A).

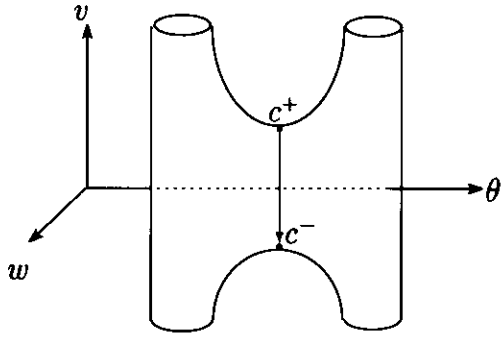

FIG.3.1 C_0 and the Homothetic solution

Let $W^s(\boldsymbol{h}(s))$ denote the stable manifold, and $W^u(\boldsymbol{h}(s))$ denote the unstable manifold. The manifolds $W^s(\boldsymbol{h}(s))$ and $W^u(\boldsymbol{h}(s))$ are both 2-dimensional. Let

$W^s(c^+)$, $W^u(c^+)$, $W^s(c^-)$ and $W^u(c^-)$ denote the invariant manifolds associated with c^+ and c^-. Then, we have the following properties by liniearization studies around the critical points (see Appendix A). $W^s(c^+)$ and $W^u(c^-)$ are 1-dimensional manifolds. $W^u(c^+)$ and $W^s(c^-)$ are 2-dimensional manifolds. Additionally,

$$W^s(\boldsymbol{h}(s)) = W^s(c^-), \quad W^u(\boldsymbol{h}(s)) = W^u(c^+). \tag{3.2.2}$$

When we pay attention to the phase flow around the critical points except for the fictitious flow, $\boldsymbol{h}(s)$ itself is included to an unstable manifold of c^+, and to a stable manifold of c^-. These two $\boldsymbol{h}(s)$ coincide with each other if $h < 0$, and they are different from each other if $h > 0$. Let W_0 be a set of all points (θ, w, v) for the homothetic solution. Then, we have

$$h < 0 \Longrightarrow W_0 \subset W^u(c^+) \cap W^s(c^-). \tag{3.2.3}$$

These relations (3.2.2) and (3.2.3) are important to discuss the structure on Σ. In the latter sections, we give such a discussion.

3.3 Various features on the surface of section

For proof of the following theorems, we use one of the original equations of motion, namely,

$$\ddot{q}_2 = -\frac{1}{q_2^2} f(\frac{q_1}{q_2}), \tag{3.3.1}$$

where a function

$$f(\xi) = \frac{\sin^2\varphi}{4} + \frac{\cos^2\varphi}{(1+\xi)^2} + \frac{\cos^2\varphi}{(1-\xi)^2} \tag{3.3.2}$$

is defined for $\xi \in [0, 1)$. The other transformed equation is used as well. The transformation is as follows.

$$Q_1 = q_1 \cos^2\varphi + q_2 \sin^2\varphi, \qquad Q_2 = q_2 - q_1. \tag{3.3.3}$$

Then, we have the equation of motion for Q_1, i.e.,

$$\ddot{Q}_1 = -\frac{1}{Q_1^2} g(\frac{Q_2}{Q_1}), \tag{3.3.4}$$

where a function

$$g(\eta) = \frac{\cos^4\varphi}{4}\left(\frac{1}{(1-\eta\sin^2\varphi)^2} + \frac{\tan^4\varphi}{(1+\eta\cos^2\varphi)^2} + \frac{8\tan^2\varphi}{(2+\eta\cos 2\varphi)^2}\right) \tag{3.3.5}$$

is defined for $\eta \in [0, 1/\sin^2\varphi)$.

Lemma 3.3.1 (Monotoneity of $f(\xi)$)

The function $f(\xi)$ is monotone increasing for $\xi \in [0, 1)$.

proof

It is trivial by a direct calculation.

$$\frac{df(\xi)}{d\xi} = \cos^2\varphi\frac{4\xi(3+\xi^2)}{(1+\xi)^3(1-\xi)^3}$$

The right-hand side is positive when $\xi \in (0, 1)$, and zero when $\xi = 0$.

Q.E.D.

Lemma 3.3.2 (Monotoneity of $g(\eta)$)

The function $g(\eta)$ is monotone increasing for $\eta \in [0, 1/\sin^2\varphi)$.

proof

We calculate the derivative of $g(\eta)$ with respect to η.

$$\frac{dg(\eta)}{d\eta} = \frac{3\eta\sin^2 2\varphi}{16(\eta_1\eta_2(\eta_1+\eta_2))^3}\Big[\eta_1^3\cos^2\varphi\big\{(\eta_1+2\eta_2)^2+3\eta_2^2\big\}+\eta_2^3\sin^2\varphi\big\{(\eta_2+2\eta_1)^2+3\eta_1^2\big\}\Big],$$

where $\eta_1 = 1+\eta\cos^2\varphi$ and $\eta_2 = 1-\eta\sin^2\varphi$. The right-hand side is positive because $\eta_1 \geq 1$ and $\eta_2 > 0$ for $\eta \in (0, 1/\sin^2\varphi)$. If $\eta = 0$, then $dg(\eta)/d\eta = 0$.

Q.E.D.

Theorem 3.3.1 (Global surface of section)

Any solution of (2.2.7) passes through Σ at a certain time.

proof

Suppose that the motion stays in 1-2-1 ejection. Then, 1-2-1 binary collisions($q_1 = 0$) occur repeatedly. The equation of motion (3.3.1) is still regular even if q_1

becomes zero. From Lemma 3.3.1, the function $f(\xi)$ is monotone increasing. Then, we have

$$0 \leq \xi < 1 \Longrightarrow f(0) \leq f(\xi).$$

Here, $f(0)$ is a positive value $(1 + 7\cos^2\varphi)/4$. Thereby,

$$\ddot{q}_2 = -\frac{1}{q_2^2} f(\frac{q_1}{q_2}) \leq -\frac{1}{q_2^2} f(0) < 0.$$

Variable q_2 moves in the field of restitutive force. Therefore, q_2 decreases until a 2-2 binary collision occurs for the future or the past. The phase point passes through Σ at a certain time on the way.

Next, suppose that the motion stays in 2-2 ejection. Then, 2-2 binary collisions($Q_2 = q_2 - q_1 = 0$) occur repeatedly. The equation of motion (3.3.4) is still regular if Q_2 becomes zero. From Lemma 3.3.2, the function $g(\eta)$ is monotone increasing. Then, we have

$$0 \leq \eta < \frac{1}{\sin^2\varphi} \Longrightarrow g(0) \leq g(\eta).$$

Here, $g(0)$ is a positive value $1/4$. Thereby,

$$\ddot{Q}_1 = -\frac{1}{Q_1^2} g(\frac{Q_2}{Q_1}) \leq -\frac{1}{4Q_1^2} < 0.$$

Variable Q_1 moves in the field of restitutive force. Therefore, Q_1 decreases until a 1-2-1 binary collision occurs for the future or the past. The phase point passes through Σ at a certain time on the way.

Q.E.D.

We would like to mention the reversibility of the system. This will be proved by direct calculations.

Lemma 3.3.3 (Reversibility of SC4BP)

Equations of motion (2.2.7) are invariant under the following transformation.

$$(s, v, w) \mapsto (-s, -v, -w)$$

This fact implies that distribution of future symbol sequences on Σ provides distribution of past symbol sequences by its rotation of π about the origin. If we define an operator $\mathcal{R}$ as reversing sequences of symbols, i.e.,

$$\mathcal{R} \ : \ [\ldots s_{-2}s_{-1}.s_0s_1s_2\ldots] \mapsto [\ldots s_2s_1s_0.s_{-1}s_{-2}\ldots],$$

then we could have another expression of the properties mentioned above.

Lemma 3.3.4 (Reversibility of Σ)

The following relation holds true for $(v, w) \in \Sigma$.

$$\mathcal{R}(\mathcal{S}(v, w)) = \mathcal{S}(-v, -w)$$

Thereby, it is sufficient to study the distribution of future sequence for the full survey of bi-infinite sequences of symbols.

Let Σ_+ denote $\{(r, \theta_c, v, w) \in \Sigma \mid w > 0\}$, Σ_- denote $\{(r, \theta_c, v, w) \in \Sigma \mid w < 0\}$, and Σ_0 denote $\{(r, \theta_c, v, w) \in \Sigma \mid w = 0\}$. As a set, Σ_0 is equal to W_0. Symbols appeared immediately after leaving Σ_+, Σ_-, Σ_0 can be predicted by the following theorem.

Theorem 3.3.2

Any solution passing through Σ_+ reaches $\theta = \pi/2$ (1-2-1 binary collision) before returning to Σ. Any solution passing through Σ_- reaches $\theta = \varphi$ (2-2 binary collision) before returning to Σ. There exists no solution passing through Σ_0 transversally.

proof

First, by using equations (2.2.2), we shall show that any solution with $\theta(\tau_0) = \theta_c$ and $u(\tau_0) > 0$ remains $u > 0$. Suppose that $u(\tau_1) = 0$ for a certain time $\tau_1 > \tau_0$ and $u(\tau) > 0$ for any time $\tau \in [\tau_0, \tau_1)$. Then $\theta(\tau_1) > \theta_c$ because $d\theta/d\tau = u$. Thereby, $du/d\tau\big|_{\tau=\tau_1} = dV(\theta(\tau_1))/d\theta > 0$. This implies that u changes from negative to positive at $\tau = \tau_1$. This is contradiction. Similarly, it is shown that any solution with $\theta(\tau_0) = \theta_c$ and $u(\tau_0) < 0$ remains $u < 0$.

By transformation (2.2.6), sign of w coincides with one of u. If $w > 0$, then $\theta(s)$ is monotone increasing by (2.2.7). If $w < 0$, then $\theta(s)$ is monotone decreasing by (2.2.7). Therefore, orbits leaving Σ_+ go to the line $\theta = \pi/2$, and orbits leaving Σ_- go to the line φ.

Σ_0 is the set of phase points of the homothetic solution $\boldsymbol{h}(s)$. Therefore, no other orbit intersect Σ_0 (see Appendix A).

Q.E.D.

If we rewrite this property and Theorem 3.3.1 in terms of symbolic dynamics, then we have the following statement.

corollary 3.3.1

$$\mathcal{S}(\Sigma_+) = [\cdots.0\cdots],$$

$$\mathcal{S}(\Sigma_0) = [\cdots.1\cdots],$$

$$\mathcal{S}(\Sigma_-) = [\cdots.2\cdots].$$

The last one is the homothetic solution itself.

If we apply Lemma 3.3.4 to corollary 3.1, then we have the following two corollaries.

corollary 3.3.2

$$\mathcal{S}(\Sigma_+) = [\cdots 2.0\cdots],$$

$$\mathcal{S}(\Sigma_0) = [\cdots 1.1\cdots],$$

$$\mathcal{S}(\Sigma_-) = [\cdots 0.2\cdots].$$

corollary 3.3.3

$$\mathcal{S}^{-1}([\cdots 0.0\cdots]) = \mathcal{S}^{-1}([\cdots 2.2\cdots]) = \emptyset$$

$$\mathcal{S}^{-1}([\cdots 1.0\cdots]) = \mathcal{S}^{-1}([\cdots 0.1\cdots]) = \emptyset$$

$$\mathcal{S}^{-1}([\cdots 1.2\cdots]) = \mathcal{S}^{-1}([\cdots 2.1\cdots]) = \emptyset$$

Especially, the second corollary shows non-existence of such a symbol sequence as it contains any of words listed above. We call such a word *un-realizable word.* Last, we have the following lemma.

Lemma 3.3.5 (Transversality)

An arbitrary orbit except for $\boldsymbol{h}(s)$ intersects Σ transversally.

proof

If a certain orbit except for $\boldsymbol{h}(s)$ makes tangent to Σ, then $d\theta/ds = 0$ leads to $w = 0$ through the second equation of (2.2.7). This is a contradiction because only $\boldsymbol{h}(s)$ take a value $w = 0$ on Σ.

$\mathcal{Q}.\mathcal{E}.\mathcal{D}.$

3.4 Geometry of Quadruple Collision Curves

Here we consider a set of initial points on Σ leading to quadruple collision. The set is denoted as $W^s(c^-) \cap \Sigma$. Obviously, $W^s(c^-) \cap \Sigma$ is a non-empty set, because the homothetic solution is included in both $W^s(c^-)$ and Σ. In addition, we have the following property.

Theorem 3.4.1 (Quadruple Collision Curves)

The set $W^s(c^-) \cap \Sigma$ consists of 1-dimensional curves.

proof

First, $\Sigma_0 = W_0$ is a 1-dimensional curve on Σ. As we mentioned above, $W^s(c^-)$ is 2-dimensional manifold. The surface of section Σ_+ and Σ_- are transversal to the flow(see Lemma 3.3.5). Therefore, if $(\Sigma_+ \cup \Sigma_-) \cap W^s(c^-)$ forms 1-dimensional curves.

$\mathcal{Q}.\mathcal{E}.\mathcal{D}.$

The intersections $W^s(c^-) \cap \Sigma$ are called *quadruple collision curves* (*QCC*, for short). The symbol sequences on QCC end up with 1 continuing endlessly. The following lemma gives the other geometric feature of QCC.

Lemma 3.4.1 (End-Points of QCC)

The end-points of a certain QCC are different points on the boundary of Σ, i.e., $\partial\text{QCC} \subset (C_0 \cap \Sigma)$.

proof

First, any end-point of QCC is not an interior point of Σ. If the end-point of QCC is an interior point of $(\Sigma \setminus \Sigma_0)$, the orbit must be tangent at that point because of the continuity of $W^s(c^-)$. This is contrary to Lemma 3.3.5. Second, we have $W^s(c^-) \supset \Sigma_0$. On the other hand, Σ_0 is also a subset of $W^u(c^+)$. Then, we have $\Sigma_0 \subset (W^s(c^-) \cap W^u(c^+))$. Therefore, $W^s(c^-)$ and $W^u(c^+)$ are connected with each other. $W^s(c^+)$ and $W^u(c^+)$ are connected on c^+. $W^s(c^+)$ is 1-dimensional curves on C_0(see Appendix A), and points on $C_0 \cap \Sigma \setminus \Sigma_0$. Then, $W^s(c^-)$ and $W^s(c^+)$ are connected with each other. Therefore, the QCC must reach $C_0 \cap \Sigma \setminus \Sigma_0$ at two different points.

$\mathcal{Q.E.D.}$

Lemma 3.4.2 (QCC as a boundary of different symbol regions)

QCC of symbol sequence $[.n_0 n_1 \cdots n_{k-1} 1 \cdots]$, $n_i = 0$ or $, 2 (i = 0, \cdots, k-1)$ is a boundary of two regions whose symbol sequences are $[.n_0 n_1 \cdots n_{k-1} n_k]$ and $[.n_0 n_1 \cdots n_{k-1} n_k']$ where $n_i (i \in \boldsymbol{Z}), n_k' \neq n_k$ are either 0 or 2.

proof

Suppose that $\mathcal{S}(\Sigma_1) = [.n_0 n_1 \cdots n_{k-1} n_k]$, and $\mathcal{S}(\Sigma_2) = [.n_0 n_1 \cdots n_{k-1} n_k']$. Here $n_k \neq n_k'$, then $n_k \neq n_{k-1}$ or $n_k' \neq n_{k-1}$. So, we assume $n_k \neq n_{k-1} = n_k'$.

There are orbits starting from $\boldsymbol{p_0} \in \Sigma_1$ and reaching $\boldsymbol{p_1} \in \Sigma \setminus \Sigma_0$ after binary collision n_{k-1} because of $n_k \neq n_{k-1}$ and corollary 3.3.2. On the other hand, QCC is connected with Σ_0. Then, there is a sequence of points on $\boldsymbol{p_0} \in \Sigma_1$ such that $\boldsymbol{p_1}$ comes close in Σ_0 as $\boldsymbol{p_0}$ comes close in QCC. When $\boldsymbol{p_0}$ goes over QCC and enter in Σ_2, the point $\boldsymbol{p_1}$ does not leave in $\Sigma \setminus \Sigma_0$ because of transversality of $\Sigma \setminus \Sigma_0$(Lemma 3.3.5), the orbits return back to binary collision $n_{k-1} = n_k'$.

$\mathcal{Q.E.D.}$

Lemma 3.4.3

There is no intersection of QCCs except for thier end-points.

Let us call QCC of Lemma 3.4.2 as *QCC of depth k*, or W_k for convenient of discussion. This is the reason to let W_0 denote the set of phase points of the homothetic solution.

There are an infinity of W_k on Σ because the depth k is unbounded. On the other hand, the end points of QCCs: ∂W_k lie on $W^s(c^+) \cap C_0 \cap \Sigma$. Namely, the possible number of ∂W_k is finite. Therefore, we can expect that an infinite number of QCCs have some common end points on $C_0 \cap \Sigma$, and that Σ is sliced by QCCs, has a stratified structure.

The boundaries of depth $k > 0$ and the detailed structure of Σ will be obtained by numerical integrations.

3.5 Escape Criteria

Using Lemma 3.3.1 and Lemma 3.3.2, we obtain the criteria for escape motion.

Theorem 3.5.1 (Sufficient Condition for 1-2-1 Escape)

(For the future)

$$v > -\frac{\sqrt{W(\theta)}}{\sin\theta\sin(\theta-\varphi)}w + \sqrt{\frac{1}{\sqrt{2}}\Big(\frac{2\sin\varphi}{\sin\theta}\Big)^3 f\Big(\frac{\tan\varphi}{\tan\theta_c}\Big)} \quad \text{when} \quad \theta_c < \theta < \frac{\pi}{2}$$

(For the past)

$$v < -\frac{\sqrt{W(\theta)}}{\sin\theta\sin(\theta-\varphi)}w - \sqrt{\frac{1}{\sqrt{2}}\Big(\frac{2\sin\varphi}{\sin\theta}\Big)^3 f\Big(\frac{\tan\varphi}{\tan\theta_c}\Big)} \quad \text{when} \quad \theta_c < \theta < \frac{\pi}{2}$$

proof

By Lemma 3.3.1, we have the following inequality.

$$0 < \xi \le \xi' < 1 \implies 0 < f(\xi) \le f(\xi') < +\infty. \tag{3.5.1}$$

Thereby, we have the following inequality from (3.3.1).

$$0 < q_1 \le q_2\xi' \implies 0 > \ddot{q}_2 \ge -\frac{1}{q_2^2}f(\xi'). \tag{3.5.2}$$

One can regard $-f(\xi')/q_2^2$ as two-body force if ξ' is a constant. If total energy is positive under two-body potential $f(\xi')/q_2$, then q_2 goes to infinity as time t increases. Hence we have the following sufficient condition for q_2 to escape while q_1 is bounded.

$$q_1 \leq q_2\xi' \quad \text{and} \quad q_2\dot{q}_2{}^2 > 2f(\xi'). \tag{3.5.3}$$

Under this condition, $\lim_{t\to\infty} q_2 = \infty$ if $\dot{q}_2 > 0$ (escape for the future), and $\lim_{t\to-\infty} q_2 = \infty$ if $\dot{q}_2 < 0$ (escape for the past). Using our new coordinates, we rewrite this condition (3.5.3) to the form as mentioned above.

$\mathcal{Q}.\mathcal{E}.\mathcal{D}.$

Theorem 3.5.2 (Sufficient Condition for 2-2 Escape)

(For the future)

$$v > \frac{\sqrt{W(\theta)}}{\cos\theta\cos(\theta-\varphi)}w + \sqrt{\frac{4\sqrt{2}}{\cos^3(\theta-\varphi)}g\Big(\frac{\tan(\theta_c-\varphi)}{\sin\varphi\cos\varphi}\Big)} \quad \text{when} \quad \varphi < \theta < \theta_c$$

(For the past)

$$v < \frac{\sqrt{W(\theta)}}{\cos\theta\cos(\theta-\varphi)}w - \sqrt{\frac{4\sqrt{2}}{\cos^3(\theta-\varphi)}g\Big(\frac{\tan(\theta_c-\varphi)}{\sin\varphi\cos\varphi}\Big)} \quad \text{when} \quad \varphi < \theta < \theta_c$$

proof

By Lemma 3.3.2 and (3.3.4), we have the following inequality.

$$0 < Q_2 \leq Q_1\eta' < \frac{1}{\sin^2\varphi} \implies 0 > \ddot{Q}_1 \geq -\frac{1}{Q_1^2}g(\eta'). \tag{3.5.4}$$

One can regard $-g(\eta')/Q_1^2$ as two-body force if η' is a constant. If total energy is positive under two-body potential $g(\eta')/Q_1$, then Q_1 goes to infinity as time t increases. Hence we have the following sufficient condition for Q_1 to escape while Q_2 is bounded.

$$Q_2 \leq Q_1\eta' \quad \text{and} \quad Q_1\dot{Q}_1{}^2 > 2g(\eta'). \tag{3.5.5}$$

Under this condition, $\lim_{t\to\infty} Q_1 = \infty$ if $\dot{Q}_1 > 0$ (for the future), $\lim_{t\to-\infty} Q_1 = \infty$ if $\dot{Q}_1 < 0$ (for the past). Recall Q_1 to be the center of masses m_1 and m_2,

and Q_2 to be the distance between m_1 and m_2. Then, 2-2 escape occurs. Using our new coordinates, we rewrite this condition (3.5.5) to the form as mentioned above.

$\mathcal{Q}.\mathcal{E}.\mathcal{D}.$

Inequalities in Theorems 3.5.1-2 in the case of equal-masses are plotted with QCM in the 3-dimensional (θ, w, v)-space (Fig.3.2). Four dark squares indicate boundaries of the inequalities. Regions above the upper squares (resp. regions below the lower squares) are escape regions for the future (resp. for the past).

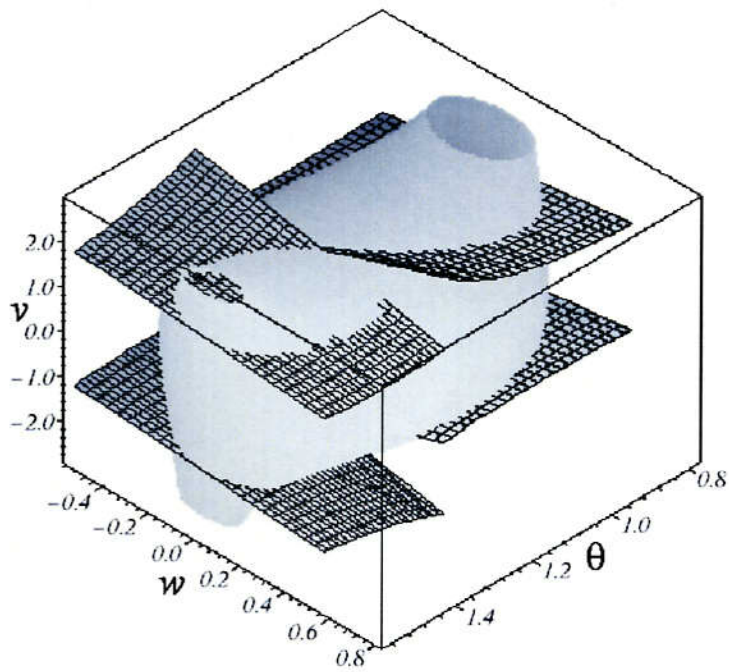

FIG.3.2: C_0 and Escape criteria for $m_1 = m_2$

As is seen in Fig.3.2, boundary squares meet at $\theta = \theta_c$. In fact, we can evaluate both escape criteria at $\theta = \theta_c$, namely the surface of section Σ.

corollary 3.5.1 (Escape Criteria on Σ)

When $\theta = \theta_c$, we have the following criteria for the future.

$$v > -\frac{\sqrt{W(\theta_c)}}{\sin\theta_c \sin(\theta_c - \varphi)} w + \sqrt{2V(\theta_c)}, \quad v > \frac{\sqrt{W(\theta_c)}}{\cos\theta_c \cos(\theta_c - \varphi)} w + \sqrt{2V(\theta_c)}$$

The following inequalities are for the past.

$$v < -\frac{\sqrt{W(\theta_c)}}{\sin\theta_c \sin(\theta_c - \varphi)} w - \sqrt{2V(\theta_c)}, \quad v < \frac{\sqrt{W(\theta_c)}}{\cos\theta_c \cos(\theta_c - \varphi)} w - \sqrt{2V(\theta_c)}$$

proof

Using the fact θ_c attains zero of $dV(\theta)/d\theta$, direct calculations give the following equalities.

$$\sqrt{\frac{1}{\sqrt{2}}\left(\frac{2\sin\varphi}{\sin\theta_c}\right)^3 f\left(\frac{\tan\varphi}{\tan\theta_c}\right)} = \sqrt{\frac{4\sqrt{2}}{\cos^3(\theta_c - \varphi)} g\left(\frac{\tan(\theta_c - \varphi)}{\sin\varphi\cos\varphi}\right)} = \sqrt{2V(\theta_c)}$$

$\mathcal{Q}.\mathcal{E}.\mathcal{D}.$

Inequalities in corollary 3.5.1 in the case of equal-masses are plotted with QCM on the surface of section Σ (Fig.3.3). The upper regions (resp. the lower regions) are escape regions for the future (resp. for the past).

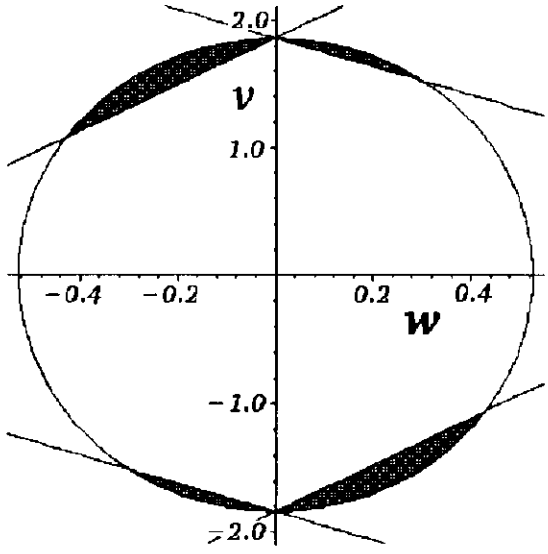

FIG.3.3: Σ and Escape criteria for $m_1 = m_2$

Chapter 4

Numerical Results

In this chapter, we state results of our numerical experiments in the case of equal-masses and negative energy. The purpose of numerical experiments is to explore the fine structure of the surface of section Σ which is not obtained by the analytical approach. First, we calculate symbol words up to 32 symbols. Due to Lemma 3.4.2, QCC can be obtained as a boundary of regions with different symbol words. Accordingly, the depth of QCC : k takes each integer from 0 to 31. Thus we have a huge number of QCCs which form some bunches. The remaining areas other than the bunches are voids where no QCC lies. The surface of section Σ is divided into bunches of QCCs and voids. Each bunch seems to have an infinity of QCCs. These areas were pointed out to be *chaotic area* by Sweatman ([55]). As our numerical results indicate, these chaotic areas have *a stratified structure* divided by QCCs.

The number of divided regions is very large but less than 2^{k+1}. This fact implies that some symbol sequences are *un-realizable*. Already we obtained a few example of such un-realizable sequences in corollary 3.3.3. Numerical calculations suggest that there exist a larger number of un-realizable sequences. In order to make sure the existence, we connect symbol words after and before Σ using *reversibility* in Lemma 3.3.5. From QCCs up to depth 12, we have a set of un-realizable words with 25 symbols. Using common properties among the un-realizable words above, we obtain a hypothesis which holds for all un-realizable words. From the hypothesis, we conjecture that a list of words are un-realizable.

Second, we examine the spatial order of QCCs which is determined by decimalizing symbol sequence. Decimalization can be done by regarding a symbol sequence as the trinary expansion of a certain real number. We plot the decimalized values versus the distance on Σ. The graph seems to be fractal, resembles to the famous devil's stair-case. In our case the graph is not monotone while the so-called devil's stair-case is monotone step function. In the case of collinear three-body problem, it is known that the order is monotone(Tanikawa et al[57]).

Third, we calculate orbits starting from voids of Σ. Orbits starting from central voids stay in the voids such that any orbits crosses two voids alternately. We calculate symbol words up to 128 of length in the void areas. Distribution of points which remain in the void after the calculations is shown. The distribution suggests the more complicated structure of Σ. Orbits starting from other voids adjacent C_0 escape after a few crossing Σ at most. We obtain the initial points leading to escape using our escape criteria(Lemma 3.5.1 and 3.5.2). Observing the results, one can see such initial points almost everywhere in Σ except for invariant regions around two points which are representative for Schubart-type periodic orbits.

Finally, we divide Σ into 12 subsets with based on QCCs, and construct the transition rule of mapping among the subsets, which give the structure of distribution of symbol sequences systematically. The rule gives possible periodic words. We directly find some periodic words by numerical survey of Σ. They coincide with some of periodic words expected from the transition rule.

4.1 Parameters of numerical calculations

Here, we describe parameters of our numerical experiments. Masses distribute homogeneously ($m_1 = m_2 = 1/2$,i.e., $\varphi = \pi/4$, $\theta_c \simeq 1.2645046604259870$, see Appendix A). Total energy is negative ($h = -1$). We regard Σ as the initial value space. We take 1000×1000 points(at least) radially and azimuthally on Σ, and obtain orbits starting from the points. Each integration was basically performed to the future until 32 binary collisions occurred at least. This gives past symbol sequences

with same length immediately, by Lemma 3.3.4. In some special experiments, the division of Σ and length of words are more detailed than above. The extrapolation method which is well-known as one of the finest numerical integrator is used as the numerical integrator.

4.2 Quadruple Collision Curves

As mentioned in Lemma 3.4.4, QCCs are obtained as boundaries between regions of different symbol sequences.

First, we obtain two regions of [.0] and [.2]. Their boundary is the homothetic solution itself. Due to the section 3.4, we call the boundary "QCC of depth 0" or W_0. We display W_0 within C_0 by the red segment in Fig.4.1. As predicted analytically, W_0 connects c^+ and c^-.

Next, we proceed the calculation for one more symbol. We obtain four regions of [.00], [.02], [.20], and [.22]. Two new boundaries are added. They are called *QCC of depth 1* or W_1. We display them within C_0 by the red curves in Fig.4.2. Similarly to these figures, the latest boundaries W_k are drawn by red curves hereafter.

Each curve of W_1 has two end points on C_0 : c^+ and the other one which we call c_1^+ if it is in Σ_+ and c_1^- if it is in Σ_-. The point c_1^+ as well as c_1^- is one of intersections $W^s(c^+)$ and Σ, i.e.,

$$c_1^+ \in W^s(c^+) \cap \Sigma, \quad c_1^- \in W^s(c^+) \cap \Sigma.$$

Similarly, each QCC has two end points on C_0 which are intersections $W^s(c^+)$ and Σ.

$$c_i^+ \in W^s(c^+) \cap \Sigma, \quad c_i^- \in W^s(c^+) \cap \Sigma, \qquad (i = 1, 2, \cdots).$$

In the case of equal-masses, it is known that there are 5 points of $W^s(c^+) \cap \Sigma_+$, and 5 points of $W^s(c^+) \cap \Sigma_-$. We give names "c_k^+, $(k = 1, 2, \cdots, 5)$" to the points $W^s(c^+) \cap \Sigma_+$ from the upper to the lower. Similarly, we give names "c_k^-, $(k = 1, 2, \cdots, 5)$" to the points on Σ_-. We describe a relation of c_i^+s or c_i^-s and the invariant manifolds $W^s(c^+)$ in Figs 4.9 and 4.10. The invariant manifold $W^s(c^+)$

consists of 2 curves winding itself around C_0 while they approach to c^+. When the fictitious time s goes to $-\infty$, $W^s(c_+)$ descends toward below and eventually winds itself around arms below. Using T as mentioned in Definition 2.3.2, we have the following relations.

$$T(c_1^+) = T(c_1^-) = c^+, \tag{4.2.1}$$

$$T(c_{i+1}^+) = c_i^-, T(c_{i+1}^-) = c_i^+, (i = 1, 2, 3), \tag{4.2.2}$$

Next, we continue to calculate the orbits, and obtain the distribution of words [.000], [.002], [.022], [.020], [.222], [.220], [.200], and [.202]. Four new boundaries are added(Fig.4.3). They are curves of W_2. In Fig.4.3, there are five end points of W_2 in $C_0 \cap \Sigma_+$ and $C_0 \cap \Sigma_-$. They are c^+, c_1^+, c_1^-, c_2^+ and c_2^-. The surface of section Σ is divided into 8 regions with QCC of depth 0 to 2. So, we expect that Σ is divided into 2^{k+1} regions with $\bigcup_{i=0}^{k} W_k$. However, W_3 does not satisfy the expectation. We display W_3 in *Fig.*4.4. One can see that Σ is divided into some regions whose number is 14, is not 2^{3+1}. The words [.0022] and [.2200] are disappeared. They are examples of unrealized word. There never exists any symbol sequence containing an unrealized word. Therefore, there never exists any orbits corresponding such a symbol sequence. A list of unrealized word was confirmed in collinear three-body problem[57]. It is the first time that unrealized words in SC4BP are discovered. It is interesting to complete the list of unrealized words. We dedicate the section 4.3 to the systematic composition of unrealized words.

Similarly to the case as above, we obtain W_4, W_5 and W_6 as shown in Figs.4.5-7. We summarize some features about distribution of QCC up to depth of 5. First, the number of QCCs in both regions Σ_+ and Σ_- is equal. Second, the number of QCC increases by one as k of W_k increases. Third, curves of W_k connect $2k+1$ pairs $(c_{n-1}^+, c_n^+), (n = 1, \cdots, k)$ and $(c_{n-1}^-, c_n^-), (n = 1, \cdots, k)$, i.e.,

$$(c_0^+, c_1^+), \quad (c_1^+, c_2^+), \quad \cdots, \quad (c_{k-1}^+, c_k^+), \qquad \text{for } k = 1, 2, \cdots, 5$$

and

$$(c_0^-, c_1^-), \quad (c_1^-, c_2^-), \quad \cdots, \quad (c_{k-1}^-, c_k^-), \qquad \text{for } k = 1, 2, \cdots, 5$$

where $c_0^+ = c_5^+ = c_0^- = c_5^- \equiv c^+$. Fourth, QCC connecting (c_0^+, c_1^+) or (c_0^-, c_1^-) are added upward. Similarly, QCCs connecting the other pairs are added outward. Thus, QCCs form bunches connecting two points of $c_i^\pm$s. The deepest QCC in any bunch always faces on surrounding voids.

Observing $W_k, (k > 6)$, we can see more complicated features about distribution of QCC. As well as the case for $k \leq 5$, the same number of QCCs are added in both sides of Σ in each depth. However, the increment is no longer one. The number of QCC of depth 6 connecting (c_0^+, c_1^+) or (c_0^-, c_1^-) increases by three, while the other QCCs connecting the other pairs increases by one.

change of depth k	$(c_0^\pm, c_1^\pm)$	$(c_1^\pm, c_2^\pm)$	$(c_2^\pm, c_3^\pm)$	$(c_3^\pm, c_4^\pm)$	$(c_4^\pm, c_5^\pm)$
$0 \to 1$	1	0	0	0	0
$1 \to 2$	1	1	0	0	0
$2 \to 3$	1	1	1	0	0
$3 \to 4$	1	1	1	1	0
$4 \to 5$	1	1	1	1	1
$5 \to 6$	3	1	1	1	1
$6 \to 7$	5	3	1	1	1
$7 \to 8$	7	5	3	1	1
$8 \to 9$	9	7	5	3	1

Table 4.1: Increments of the number of QCC faced on surrounding voids.

The increments are summarized in Table.4.1. Obviously, a simple rule can be read in Table.4.1. On the other hand, the spatial order of QCCs in any bunch is not simple, while the order in collinear tree-body problem is monotone if symbol sequences are regarded as a binary expansion of a certain real number. Let us observe the spatial order of QCCs in a bunch (see Fig.4.8 and Table4.2).

We draw a segment $\mathbf{PQ}$ normal to the bunch connecting c^+ and c_1^- in Fig.4.8 where QCCs of depth up to 7 are appeared. The spatial order of QCCs along the segment from $\mathbf{P}$ to $\mathbf{Q}$ is described in Table4.2. As is seen in Table4.2, the spatial order of QCCs is complicated.

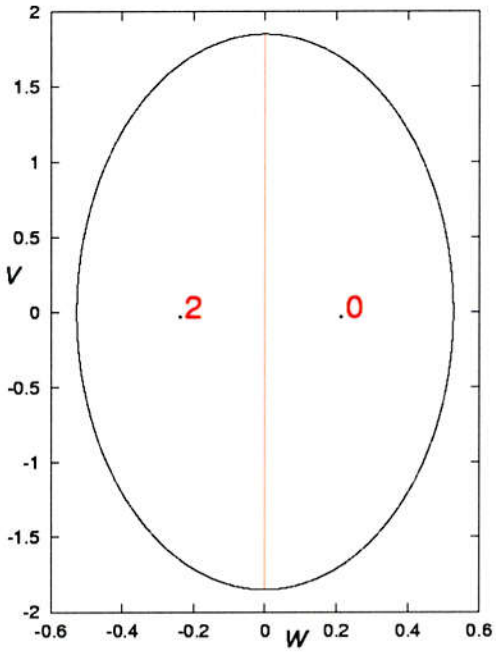

FIG.4.1: W_0 within C_0

The central vertical segment is W_0.

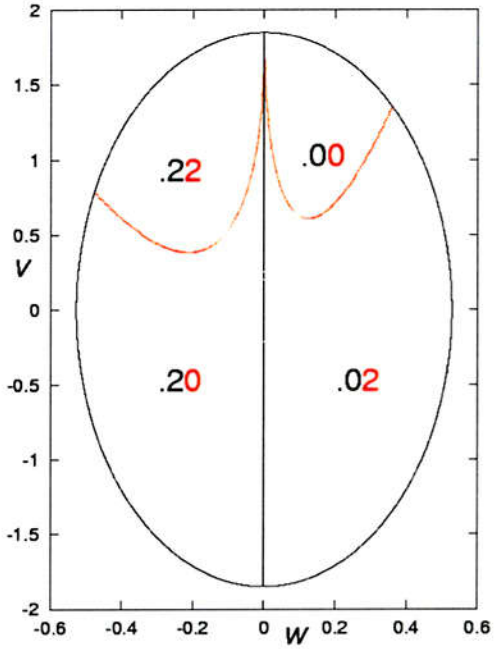

FIG.4.2: $W_0 \cup W_1$ within C_0

Two red u-shaped curves are W_1.

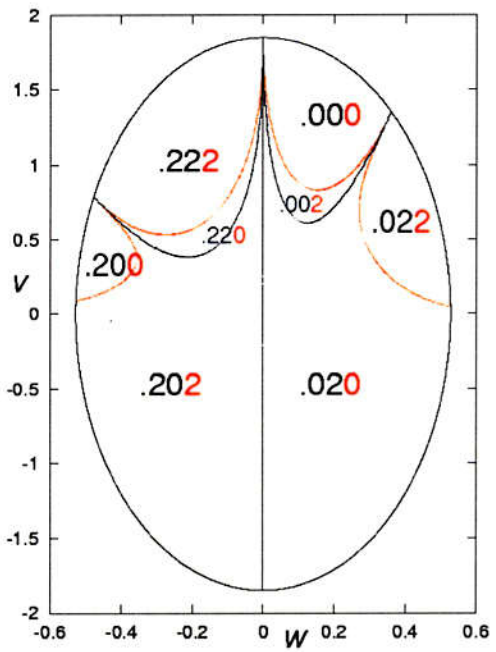

FIG.4.3: C_0 and $\bigcup_{k=0}^{2} W_k$

W_2 is shown by red curves.

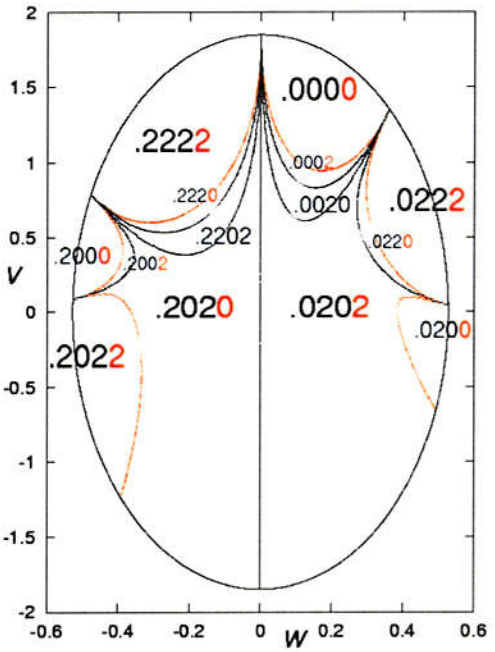

FIG.4.4: C_0 and $\bigcup_{k=0}^{3} W_k$

W_3 is shown by red curves.

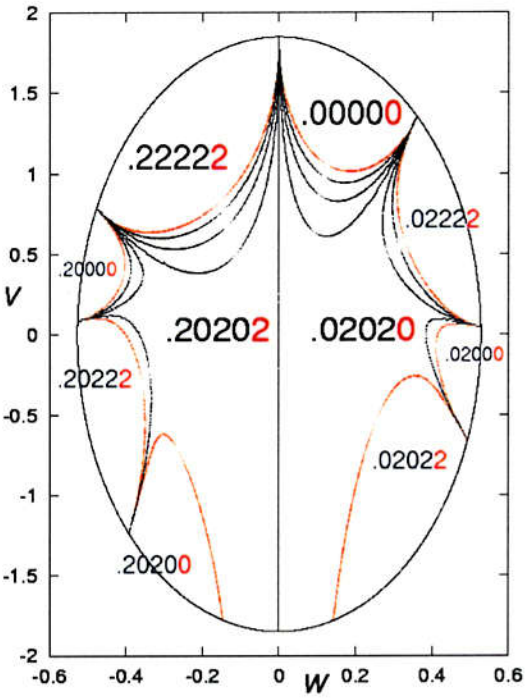

FIG.4.5 : C_0 and $\bigcup_{k=0}^{4} W_k$

W_4 is shown by red curves.

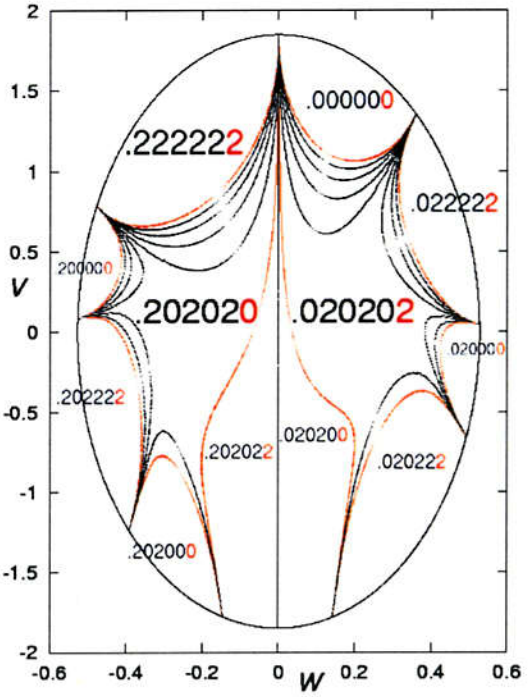

FIG.4.6 : C_0 and $\bigcup_{k=0}^{5} W_k$

W_5 is shown by red curves.

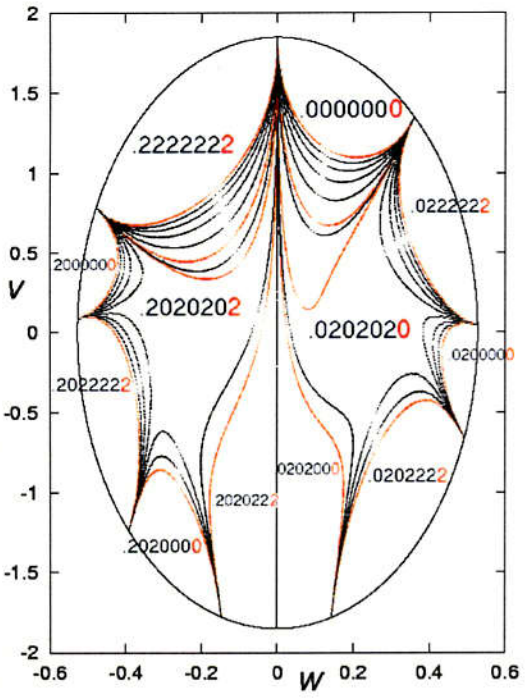

FIG.4.7 : C_0 and $\bigcup_{k=0}^{6} W_k$

W_6 is shown by red curves.

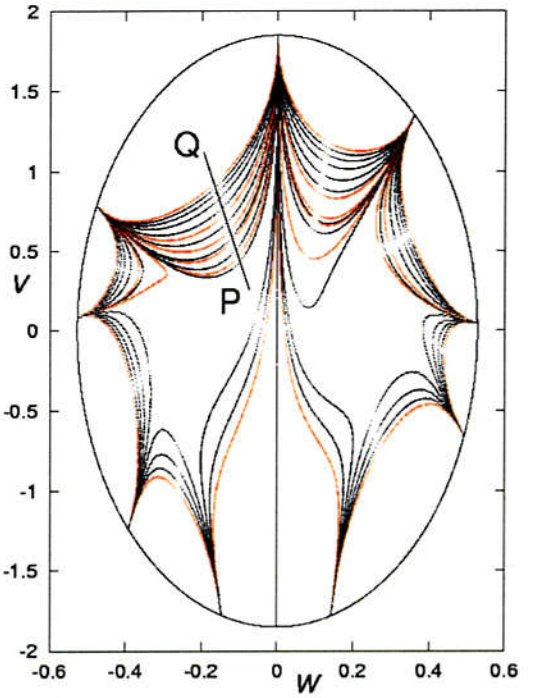

FIG.4.8 : C_0 and $\bigcup_{k=0}^{7} W_k$

W_7 is shown by red curves. Words of W_k along a segment **PQ** is shown in Table.4.2.

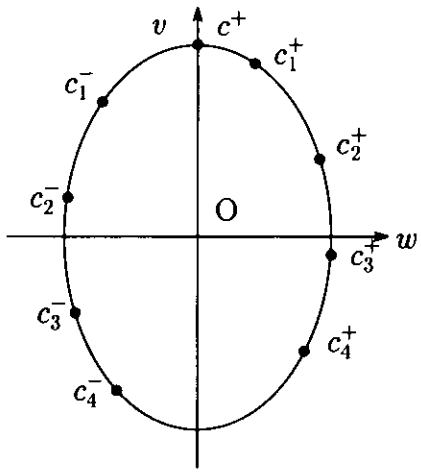

FIG.4.9 : Points c_k^+s and c_k^-s and C_0

Schematic view of the distribution in the case of equal masses is given.

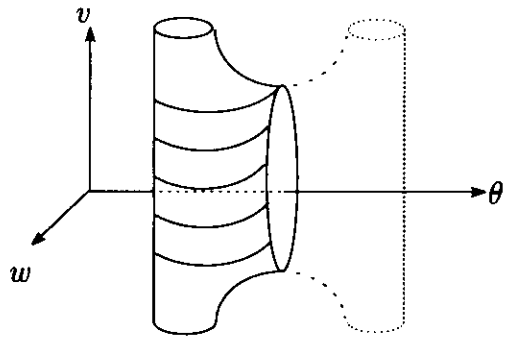

FIG.4.10 : Perspective of $W^s(c^+)$ and C_0

Schematic view in the case of equal masses is given. See [47].

k	Word	k	Word
(Q, the upper void)	[.22222222]	7	[.22020221]
7	[.22222221]	6	[.22020211]
6	[.22222211]	7	[.22020201]
5	[.22222111]	1	[.21111111]
4	[.22221111]	7	[.20202001]
3	[.22211111]	6	[.20202011]
7	[.22202021]	(P, the central void)	[.20202020]
2	[.22111111]		

Table 4.2: The spatial order of QCCs along the segment **PQ** in Fig.4.8

It is difficult to find any rule in the spatial order of QCCs. Then, We adopt the idea of ternary expansion of real numbers. Any real number can be expressed by three digits in a ternary expansion: 0,1, and 2. A symbol sequence can be regarded as a ternary expansion of a certain real number. Thereby, we transform the symbol words obtained numerically to the real numbers. We dedicate the section 4.7 to the study of the spatial order of QCCs by the method of ternary expansion.

4.3 Un-realizable Sequences

Using Lemma 3.3.3, we can construct past sequences from future sequences. Namely, rotation of the distribution of future sequences by π gives the distribution of past sequences. Accordingly, to combine future sequences and past sequences gives bi-infinite sequences.

We already have the distribution of future words by numerical integrations (Figs.1-7). Here, we rotate Fig.2 by π (Fig.11). Two QCCs of depth 1 are plotted in Fig.2. So past image of them appear

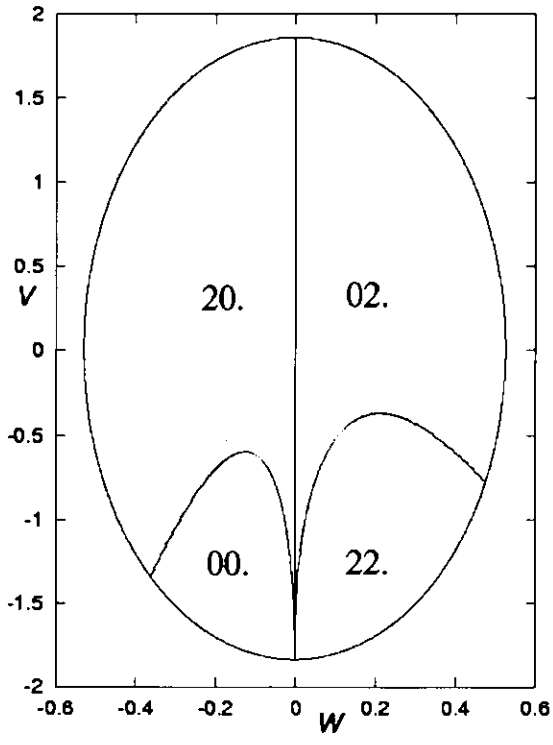

FIG.4.11: Past QCCs up to depth 2

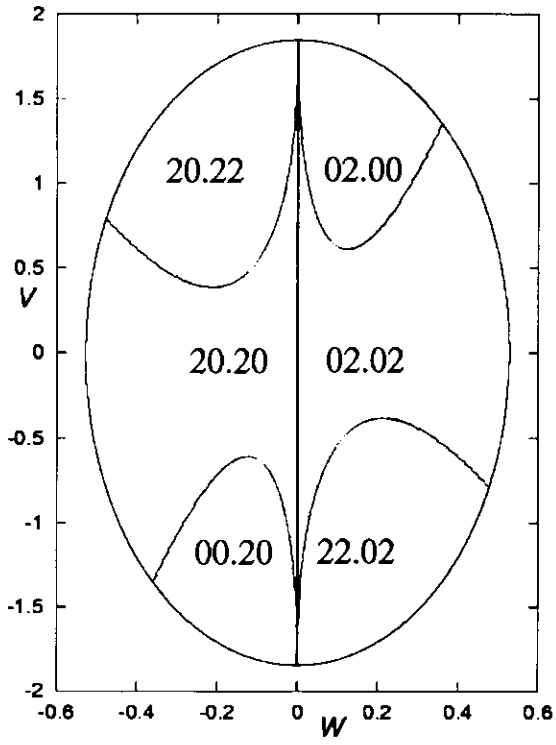

FIG.4.12: Super-imposition of Fig.4.2 and Fig.4.11

First, see Fig.4.2. There are two QCCs of depth 1. We rotate the figure by π(Fig.4.11). There are four regions of past words: [00.], [02.], [20.] and [22.]. It is observed in Fig.4.12 that regions of [00.] and [22.] have no intersection with re-

gions of [.00] and [.22]. In other words,

$$\mathcal{S}^{-1}\big([00.]\big) \cap \mathcal{S}^{-1}\big([.22]\big) = \mathcal{S}^{-1}\big([22.]\big) \cap \mathcal{S}^{-1}\big([.00]\big) = \emptyset.$$

Namely, [00.22] and [22.00] are un-realizable words.

$$\mathcal{S}^{-1}\big([00.22]\big) = \mathcal{S}^{-1}\big([22.00]\big) = \emptyset.$$

This means non-existence of any sequence which contains [0022] or [2200].

Similarly, we examine the distribution of symbol words up to depth 13. Then, we obtain a list of un-realizable words (Table.4.3).

Order	Family I	Family II	Family III	Family III'
0			[0022]	[2200]
1	[0(02)00]	[22(02)2]	[00(20)22]	[22(02)00]
2				
3	$[0(02)^3 00]$	$[22(02)^3 2]$	$[00(20)^3 22]$	$[22(02)^3 00]$
4	$[0(02)^4 00]$	$[22(02)^4 2]$		
5			$[00(20)^5 22]$	$[22(02)^5 00]$
6	$[0(02)^6 00]$	$[22(02)^6 2]$	$[00(20)^6 22]$	$[22(02)^6 00]$
7				
8	$[0(02)^8 00]$	$[22(02)^8 2]$	$[00(20)^8 22]$	$[22(02)^8 00]$
9	$[0(02)^9 00]$	$[22(02)^9 2]$		
10			$[00(20)^{10} 22]$	$[22(02)^{10} 00]$
11	$[0(02)^{11} 00]$	$[22(02)^{11} 2]$	$[00(20)^{11} 22]$	$[22(02)^{11} 00]$

Table 4.3: un-realizable words by Numerical Observations

Let us construct rules observed over distribution of QCCs up to 13th in order to obtain the un-realizable words in general. We aim to give a conjecture on the un-realizable words under assumption that the rules holds true for distribution of all QCCs.

When we add QCC until the depth exceeds 30, we have the follwing result (Fig.4.13). There is no QCC in some void regions with letters "A" to "L". QCCs seem to accumulate toward the boundaries of void regions. According to these accumulation curves of QCCs, we divide Σ into 12 regions (Fig.4.14).

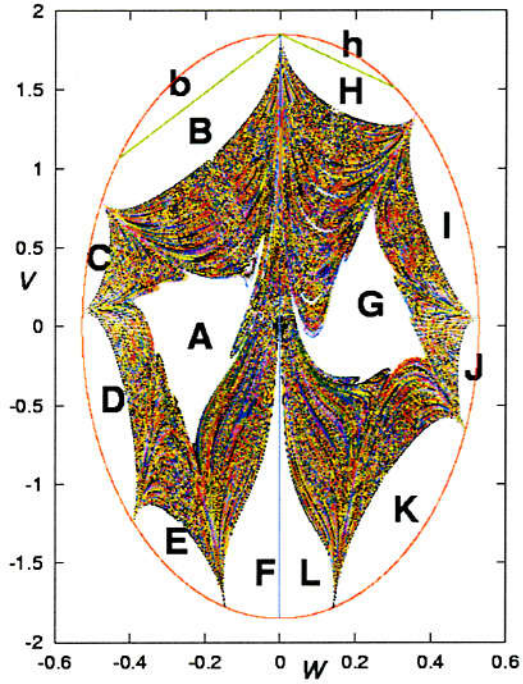

FIG.4.13: QCCs on Σ

QCC up to 31st are plotted. Letters A to N explained in Table 4.7.

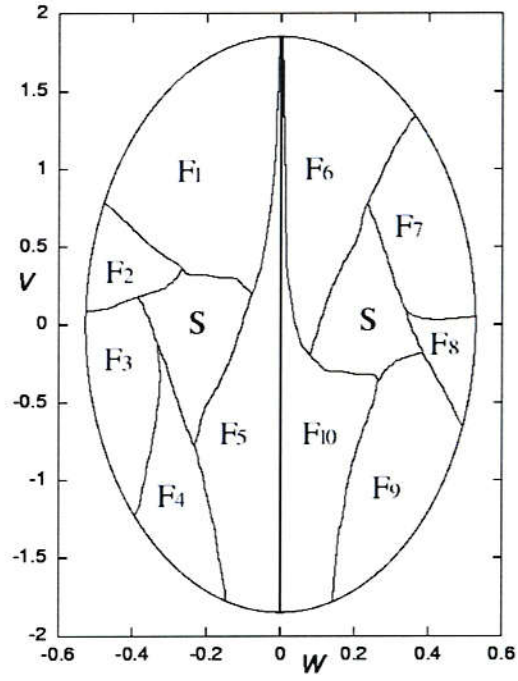

FIG.4.14: Division of Σ

Region "S" is the stable region in Fig.4.13. Each of regions F_i includes a bunch of QCCs and a void.

We regard a void and its neighboring bunch of QCCs as one region. Then, we have such 10 pairs. In addition, we regard the central two voids "S" as independent regions. We express them by $F_i, (i = 1, 2, \ldots, 10)$, "S". Similarly, a division of past images of Σ : "P_i" can be obtained. We give a list of intersection of pairs (F_i, P_j). Regions B_k's are shown in the right of Fig.4.15.

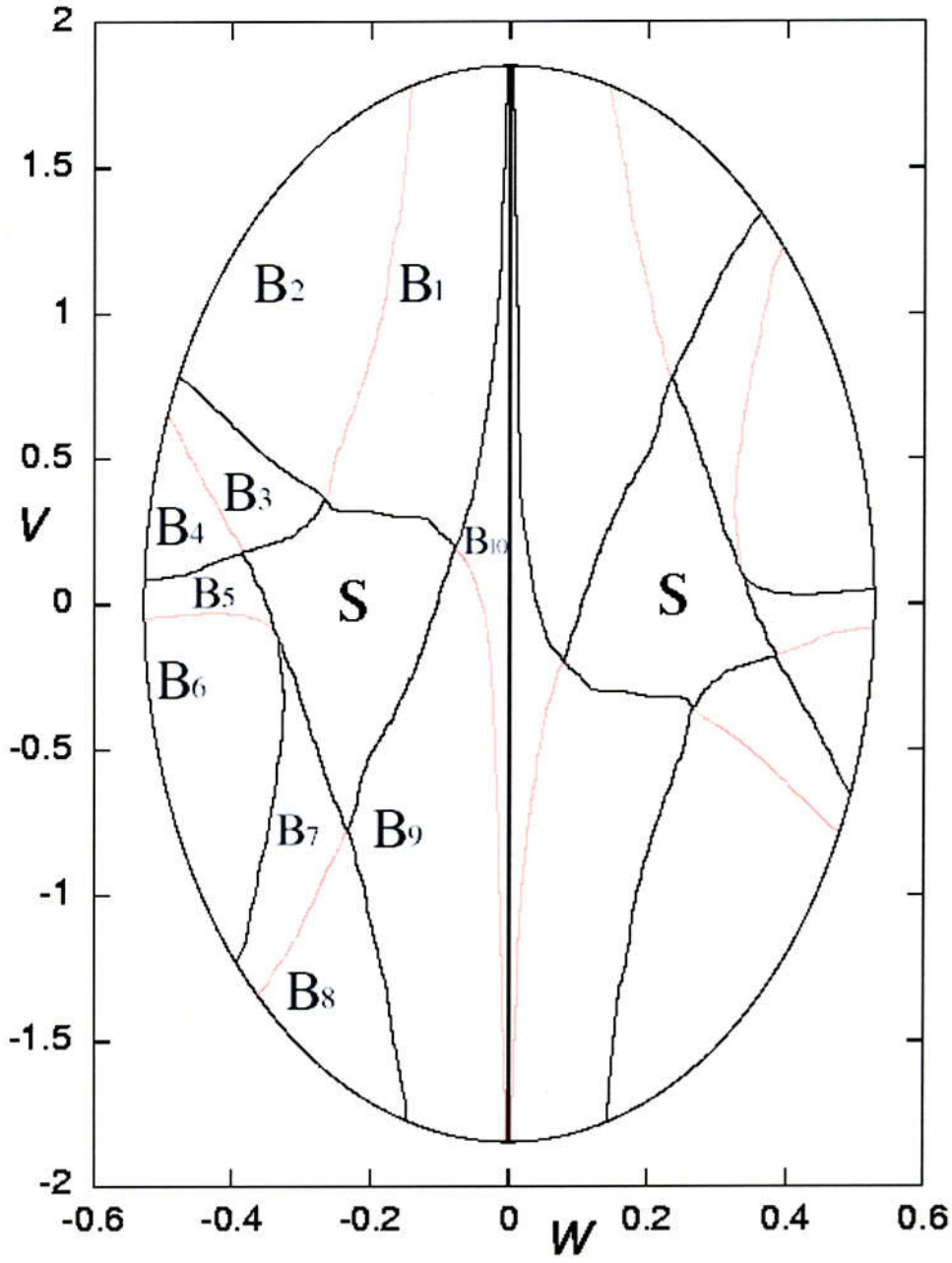

FIG.4.15: The division by F_i's and their reverse image

Regions B_1 to B_{10} are intersections of F_i $(1 \leq i \leq 5)$ and the reverse images $\mathcal{R}(F_i)$ $(6 \leq i \leq 10)$.

	P_6	P_7	P_8	P_9	P_{10}
F_1	$\emptyset$	$\emptyset$	$\emptyset$	B_2	B_1
F_2	$\emptyset$	$\emptyset$	B_4	B_3	$\emptyset$
F_3	$\emptyset$	B_6	B_5	$\emptyset$	$\emptyset$
F_4	B_8	B_7	$\emptyset$	$\emptyset$	$\emptyset$
F_5	B_9	$\emptyset$	$\emptyset$	$\emptyset$	B_{10}

Table 4.4: Intersections of F_i's and P_j's

S	Neighboring Regions: F_i, $(i = 1, 2, \ldots, 5)$				
$[.(02)^N0]$	$[.(02)^N2]$	$[.(02)^{N-1}00]$	$[.(02)^{N-1}2]$	$[.(02)^{N-2}00]$	$[.(02)^{N-2}2]$
$[.(02)^N]$	$[.(02)^{N-1}00]$	$[.(02)^{N-1}2]$	$[.(02)^{N-2}00]$	$[.(02)^{N-2}2]$	$[.(02)^{N-3}00]$
$[.(20)^N2]$	$[.(20)^N0]$	$[.(20)^{N-1}22]$	$[.(20)^{N-1}0]$	$[.(20)^{N-2}22]$	$[.(20)^{N-2}0]$
$[.(20)^N]$	$[.(20)^{N-1}22]$	$[.(20)^{N-1}0]$	$[.(20)^{N-2}22]$	$[.(20)^{N-2}0]$	$[.(20)^{N-3}22]$

Table 4.5: Words in the invariant region and the neighboring regions are listed above.

There are some pairs whose intersection is empty. They give a list of un-realizable words. Here again let us see QCCs in Figs.4.1-7. A certain number of the highest order of QCC (in one figure) are pinned to C_0. One of the highest QCC is faced on the invariant region. It is laid along one of fractal bunches toward the invariant region. The other highest QCC is embedded in other bunches. The order of five QCCs faced on the invariant region are different from each other. This suggests that the orders of QCCs range from $N-4$ to N if N is the highest order in one figure. We have symbol sequences up to 31 depth in Fig.4.13. In the region S, the symbol sequences are $[.(20)^{16}]$. Then symbol sequences in the neighboring bunches include $[.(20)^{15}22]$, $[.(20)^{15}0]$, $[.(20)^{14}22]$, $[.(20)^{14}0]$ and $[.(20)^{13}22]$. Thereby, let us give the following assumption.

Allocation of these words to F_i's changes with period 5, which we display in

Length	N	F_1	F_2	F_3	F_4	F_5	F_6	F_7	F_8	F_9	F_{10}
$2N$	$5k+1$	w_2	w_6	w_5	w_4	w_3	v_2	v_6	v_5	v_4	v_3
$2N+1$	$5k+1$	w_2	w_1	w_5	w_4	w_3	v_2	v_1	v_5	v_4	v_3
$2N$	$5k+2$	w_4	w_3	w_2	w_6	w_5	v_4	v_3	v_2	v_6	v_5
$2N+1$	$5k+2$	w_4	w_3	w_2	w_1	w_5	v_4	v_3	v_2	v_1	v_5
$2N$	$5k+3$	w_6	w_5	w_4	w_3	w_2	v_6	v_5	v_4	v_3	v_2
$2N+1$	$5k+3$	w_1	w_5	w_4	w_3	w_2	v_1	v_5	v_4	v_3	v_2
$2N$	$5k+4$	w_3	w_2	w_6	w_5	w_4	v_3	v_2	v_6	v_5	v_4
$2N+1$	$5k+4$	w_3	w_2	w_1	w_5	w_4	v_3	v_2	v_1	v_5	v_4
$2N$	$5k+5$	w_5	w_4	w_3	w_2	w_6	v_5	v_4	v_3	v_2	v_6
$2N+1$	$5k+5$	w_5	w_4	w_3	w_2	w_1	v_5	v_4	v_3	v_2	v_1

Table 4.6: Allocation of words to F_i's ($i = 1, 2, \ldots, 10$), where $w_1 = [.(20)^N 0]$, $w_2 = [.(20)^{N-1}22]$, $w_3 = [.(20)^{N-1}0]$, $w_4 = [.(20)^{N-2}22]$, $w_5 = [.(20)^{N-2}0]$, $w_6 = [.(20)^{N-3}22]$, $v_1 = [.(02)^N 0]$, $v_2 = [.(02)^{N-1}22]$, $v_3 = [.(02)^{N-1}0]$, $v_4 = [.(02)^{N-2}22]$, $v_5 = [.(02)^{N-2}0]$, and $v_6 = [.(02)^{N-3}22]$

Table.4.6 with an appropriate positive integer k.

Definition 4.4.1 (Winding Number)

Winding number of $[0(02)^k 00]$ or $[22(02)^k 2]$ is said to be k. Winding number of $[00(20)^k 22]$ or $[22(02)^k 00]$ is said to be $k + \frac{1}{2}$.

Numerical Conjecture (Un-realizable Sequence)

There never exist symbol sequences containing words whose winding numbers are

$$5k + \frac{1}{2}, \quad , 5k+1, \quad 5k+1+\frac{1}{2} \quad 5k+3, \quad 5k+3+\frac{1}{2}, \quad 5k+4,$$

where $k \geq 0$ is an integer.

4.4 Fractals

As seen in Fig.4.13, there is a densely stratified structure of QCCs. As we pointed out in the section 4.2, the geometrical order of QCCs is not monotonic. In order to quantify the geometrical order, we decimalize symbols words in the folwoing manner. For a certain symbol word $\boldsymbol{s} = (.s_0 s_1 s_2 \dots s_n)$, *decimalized value of* $\boldsymbol{s}$ is given by

$$D(s) = D(.s_0 s_1 s_2 \dots s_n) = \sum_{k=0}^{n} s_k (\frac{1}{3})^k.$$

In *decimalization of symbol words*, we regard symbol words as the trinary expansion of real numbers. By decimalization, a certain real number is corresponded to each point on Σ. We make a 3-D plot of decimalized values of symbol sequences versus $(w, v) \in \Sigma$ (see Fig.4.16). The surfaces are of a stepwise function, whose structure is difficult to understand even if the point of view is changed. As decimlized values along a QCC is constant, however, it is sufficient to see the surface perpendicularly to QCCs. As we mentioned in the previous section, subregions F_is resemble each other. As each region F_i has a stratified structure of QCCs, it is sufficient to take a vertical section of the surface above the subregions F_is

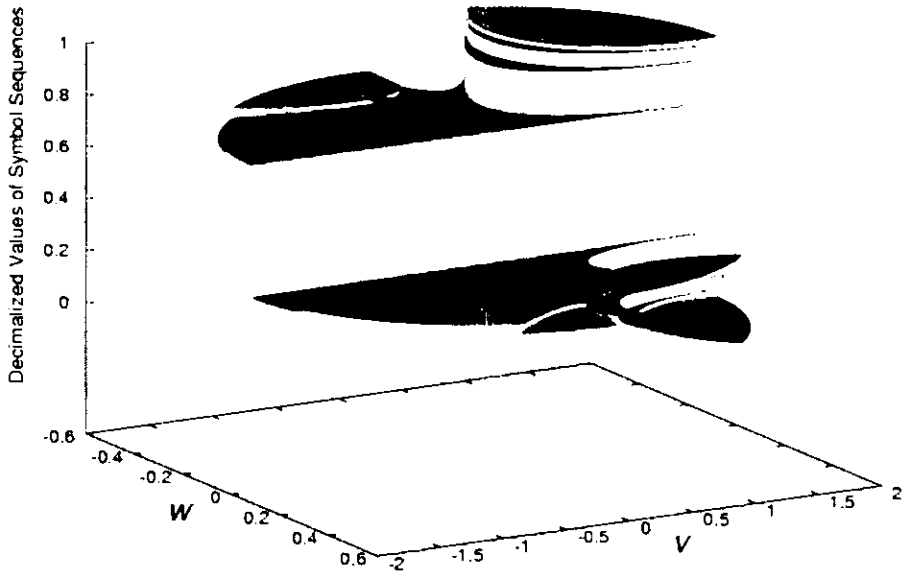

FIG.4.16: 3D-plot of Decimalized Values of Symbol Sequences

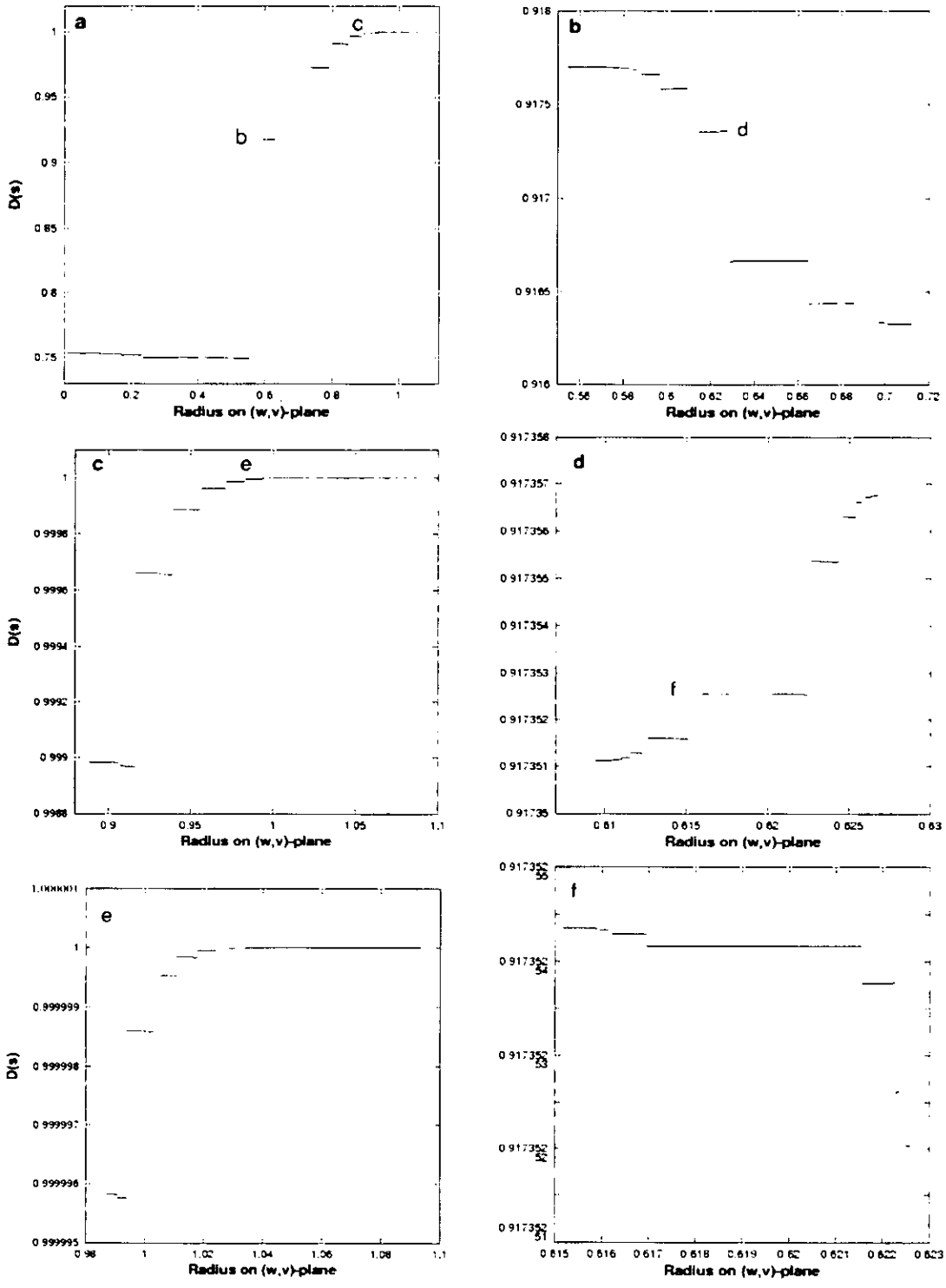

FIG.4.17 : A vertical section of Fig.4.16

The top left figure denoted by letter **a** is the vertical section along **PQ**. Figures denoted by letters **b** to **f** are enlargements of steps in figures **a** to **d**.

So let us deote our attention to one of them: F_1. We take a vertical section of the surface(Fig.4.16) along the segment **PQ** which is taken on F_1, shown in Fig.8. The vertical section is shown in Fig.4.17a. As seen in Fig.4.17a, it is an increasing and disconnected multi-step function. However, it seems to be decreaing in a step b. An enlargement of step b is given in Fig.4.17b. In fact, step b is a decreasing function. Contrary to b, a step d seems to be increasing. An enlargement of d is given in Fig.4.17d. An enlargement of f in Fig.4.17d is given in Fig.4.17f. As is seen in the figures, increasing property and decreasing property are observed alternately.

Additionally, self-similarlity is seen in Figs 4.17s. Look at Fig.4.17b, 4.17d and 4.17f, they resemble each other (except for reversal) and have three broad substeps at center and both sides. Enlargements near by the broad steps are shown in Fig.4.17c and 4.17e. It looks to have an infinity of narrow steps between the broad steps. Thus, the surface of decimalization looks a fractal: *strange devil's staircase*, which is different from the ordinary devil's staircase.

4.5 Transition rule among the subregions

In this section, we aim to establish the transition rule by the mapping T among regions divided appropriately. We have two ways of partitioning Σ. In the both ways, Σ can be divided into 12 regions. As mentioned the detail in the section 4.3, we divide Σ by the deeper QCCs. The number of QCCs increases as k increases. Numerical observation suggests that QCCs accumulate toward the void regions. Using the boundary to which QCCs accumulate, Σ can be divided (see Fig.4.13).

We have another idea of partitioning Σ. Here, we divide Σ by lower depth of QCCs. There are 9 end points of QCCs on $C_0 \cap \Sigma$. When the depth of QCCs k is less than 5, only c^+, c_k^+ and c_k^- are connected by QCCs. All end points are connected by some QCCs when $k \geq 5$. Based on this fact, we divide Σ into 12 regions which are denoted by letters I_1 to I_{12} (see Fig. 4.18). By T, each region is mapped on the other region(s) (see Fig.4.19-4.30). The transition rule among I_k $(k = 1, 2, \cdots, 12)$ will be given in the form of directed graph (see Fig.4.31). Another way of expression

for the transition rule is a transition matrix. This gives an easy way to find possible periods of some periodic points. The following section 4.7 is dedicated to the study of periodic points.

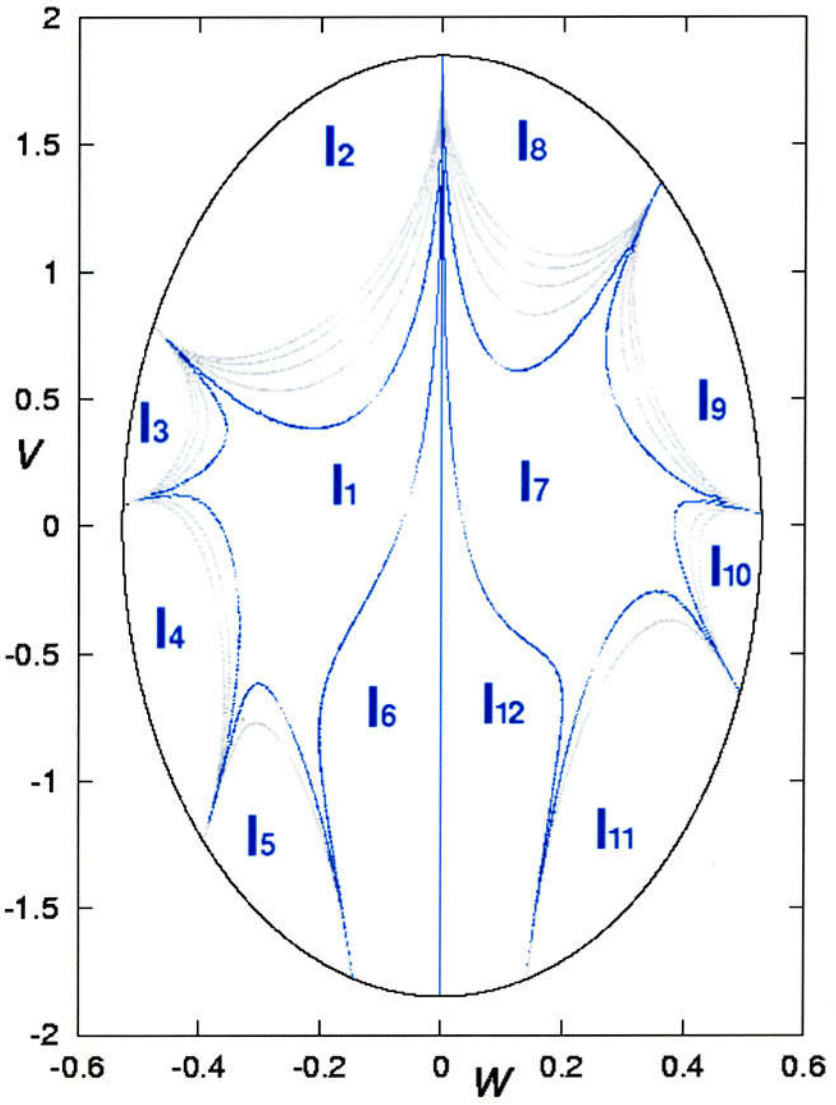

FIG.4.18: Division of Σ

Σ is devided into 12 regions by blue curves of QCCs. Each region is denoted by letters "I_1" to "I_{12}". The boundaries beween $I_1 - I_2$ or $I_7 - I_8$ are W_1. The boundaries beween $I_1 - I_3$ or $I_7 - I_9$ are of W_2. The boundaries beween $I_1 - I_4$ or $I_7 - I_{10}$ are of W_3. The boundaries beween $I_1 - I_5$ or $I_7 - I_{11}$ are of W_4. The boundaries beween $I_1 - I_6$ or $I_7 - I_{12}$ are of W_5. The boundaries beween $I_6 - I_{12}$ is of W_0.

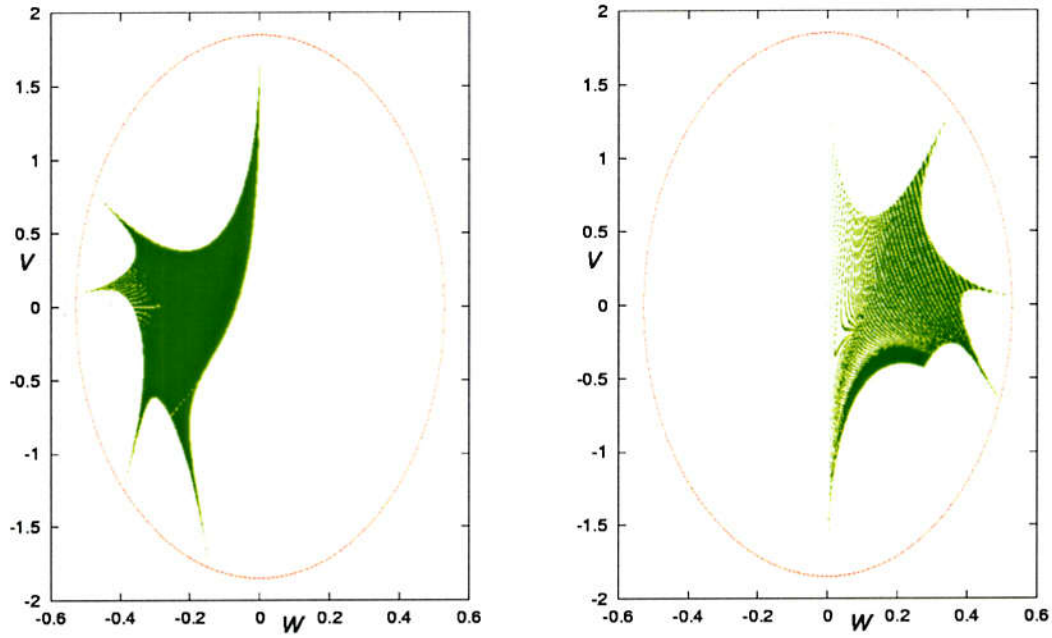

FIG.4.19: Regions I_1 and $T(I_1)$

Region I_1 is displayed in the left. The image $T(I_1)$ is displayed in the right. $T(I_1)$ intersects I_7 and I_{12}.

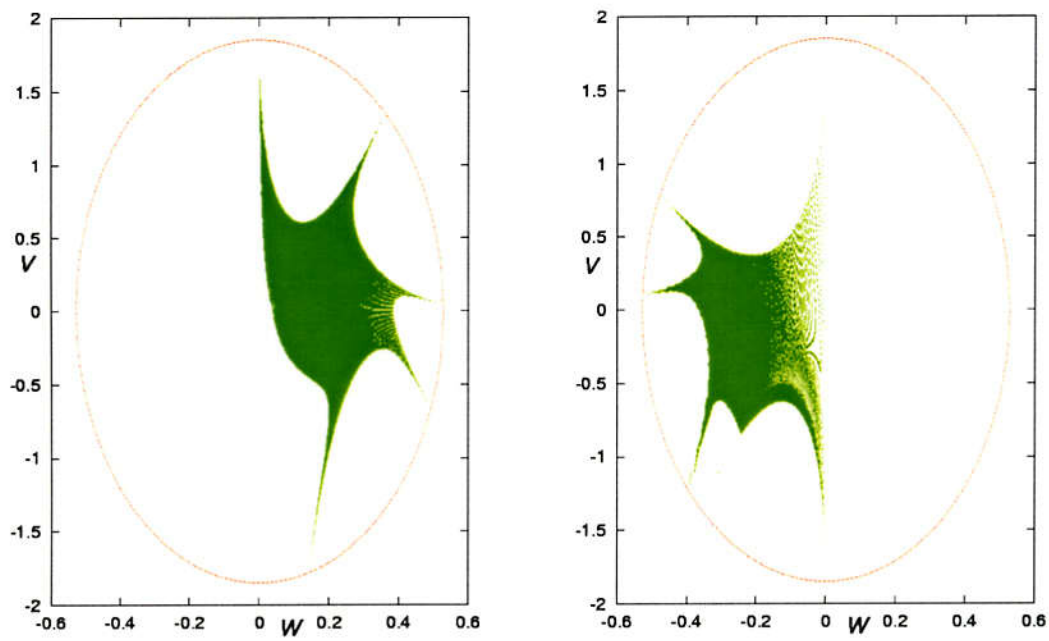

FIG.4.20: Regions I_7 and $T(I_7)$

Region I_7 is displayed in the left. The image $T(I_7)$ is displayed in the right. $T(I_7)$ intersects I_1 and I_6.

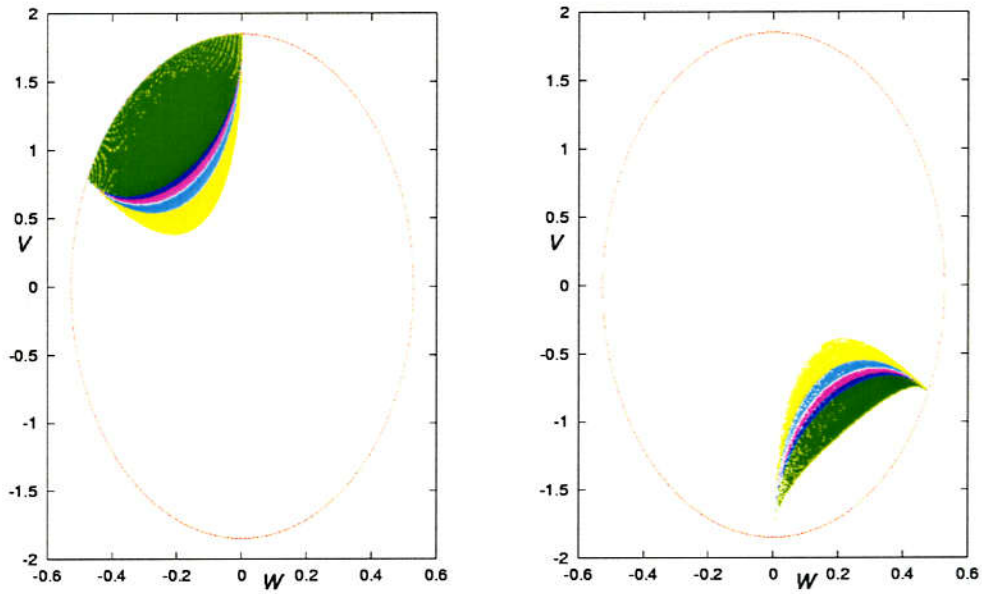

FIG.4.21: Regions I_2 and $T(I_2)$

Region I_2 (left) except for the immediate escapers is mapped on I_7, I_{11} and I_{12}. The void region between the image $T(I_2)$ (right) and C_0 denotes the immediate escapers to the past.

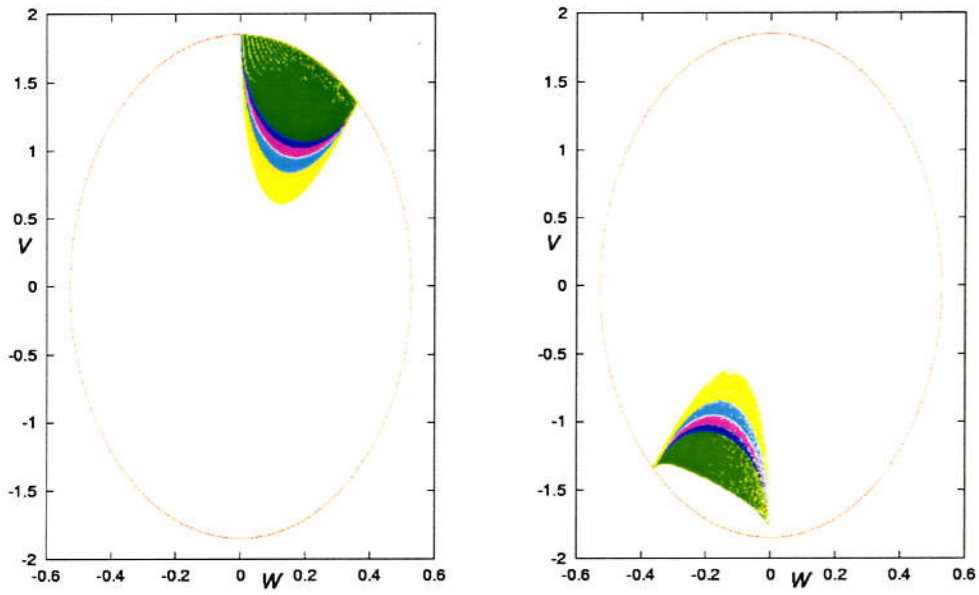

FIG.4.22: Regions I_8 and $T(I_8)$

Region I_8 (left) except for the immediate escapers is mapped on I_1, I_5 and I_6. The void region between the image $T(I_8)$ (right) and C_0 denotes the immediate escapers to the past.

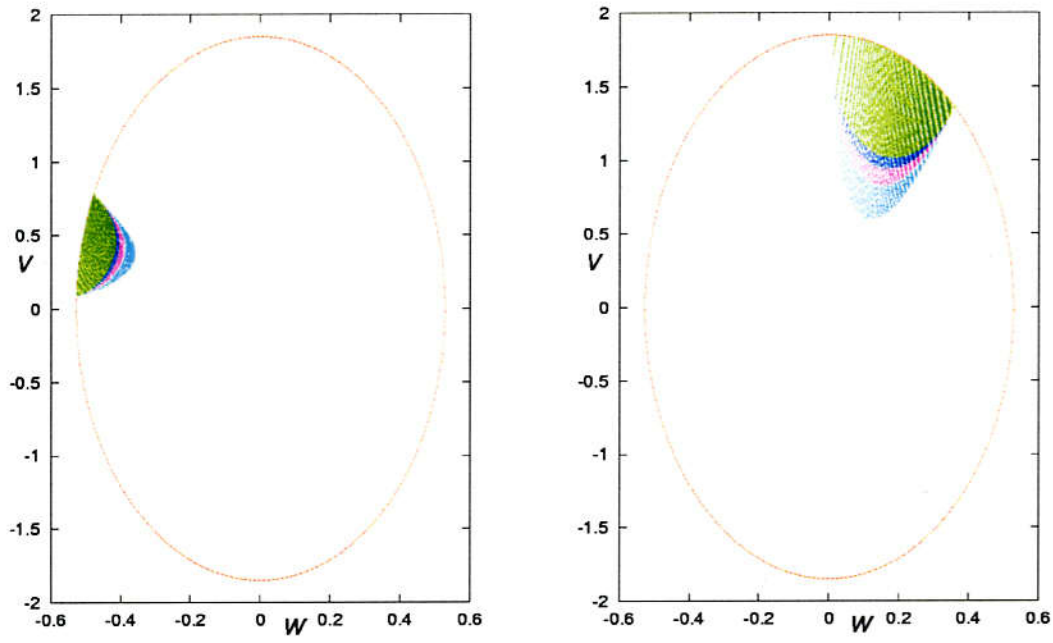

FIG.4.23: Regions I_3 and $T(I_3)$

Region I_3 is displayed in the left. The image $T(I_3)$ is displayed in the right. $T(I_3)$ is mapped onto I_8.

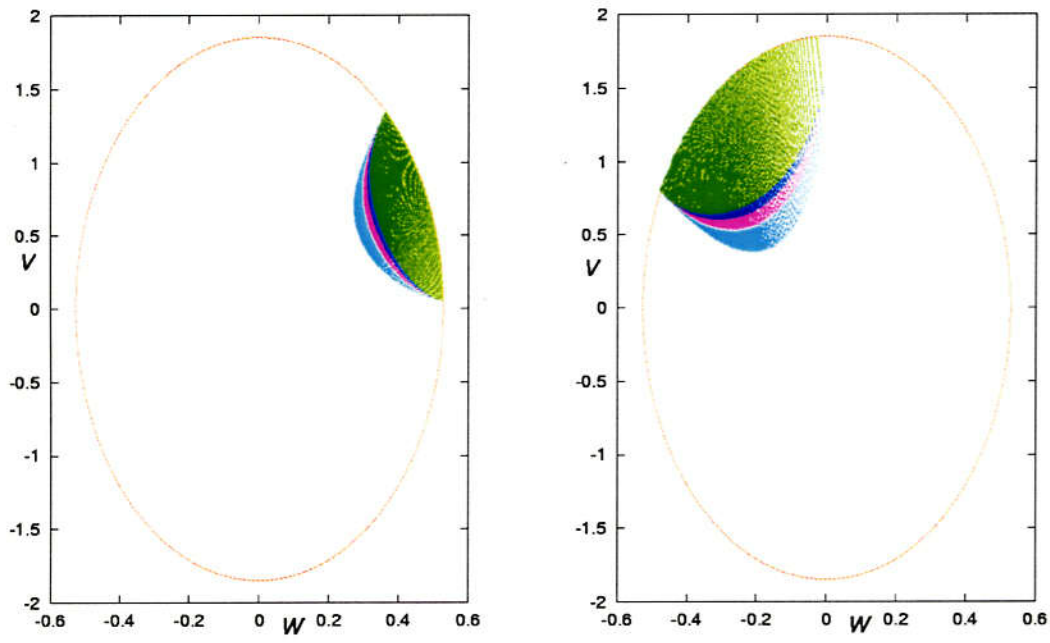

FIG.4.24: Regions I_9 and $T(I_9)$

Region I_9 is displayed in the left. The image $T(I_9)$ is displayed in the right. $T(I_9)$ is mapped onto I_2.

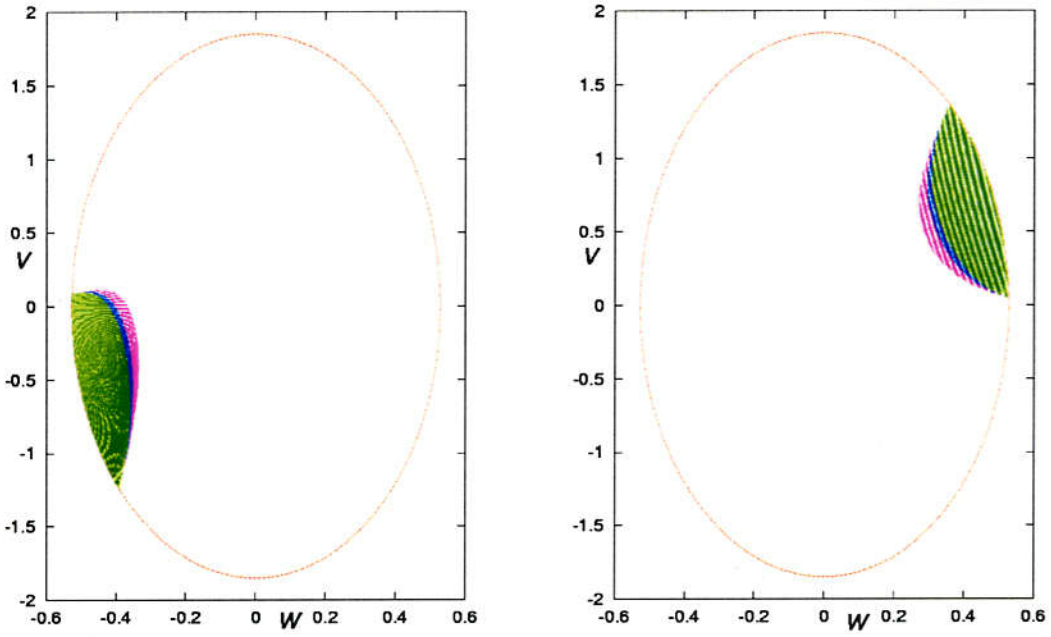

FIG.4.25: Regions I_4 and $T(I_4)$

Region I_4 is displayed in the left. The image $T(I_4)$ is displayed in the right. $T(I_4)$ is mapped onto I_9.

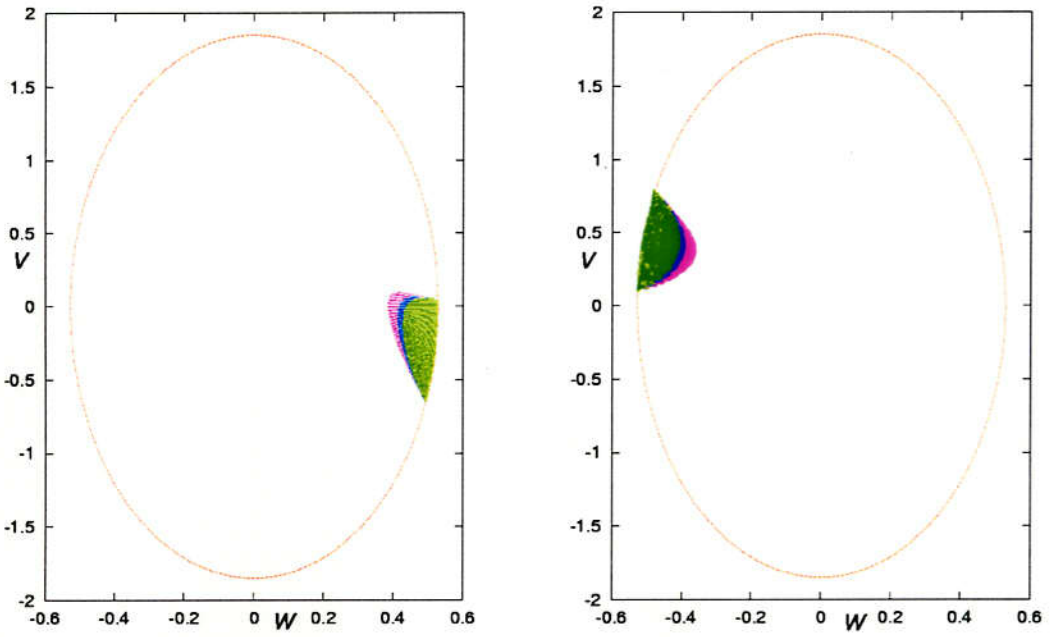

FIG.4.26: Regions I_{10} and $T(I_{10})$

Region I_{10} is displayed in the left. The image $T(I_{10})$ is displayed in the right. $T(I_{10})$ is mapped onto I_3.

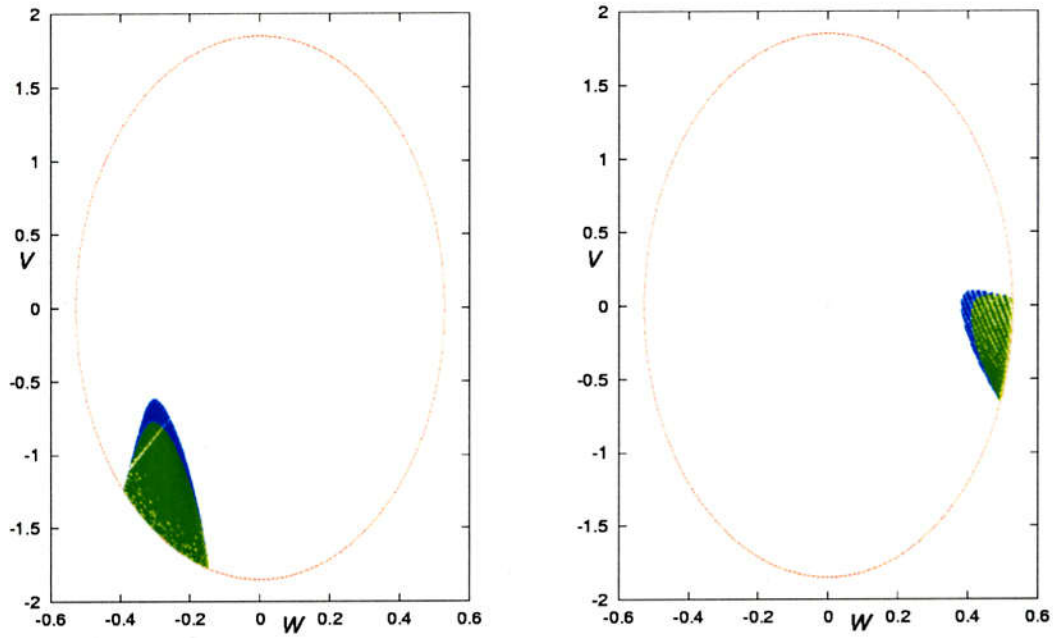

FIG.4.27: Regions I_5 and $T(I_5)$

Region I_5 is displayed in the left. The image $T(I_5)$ is displayed in the right. $T(I_5)$ is mapped onto I_{10}.

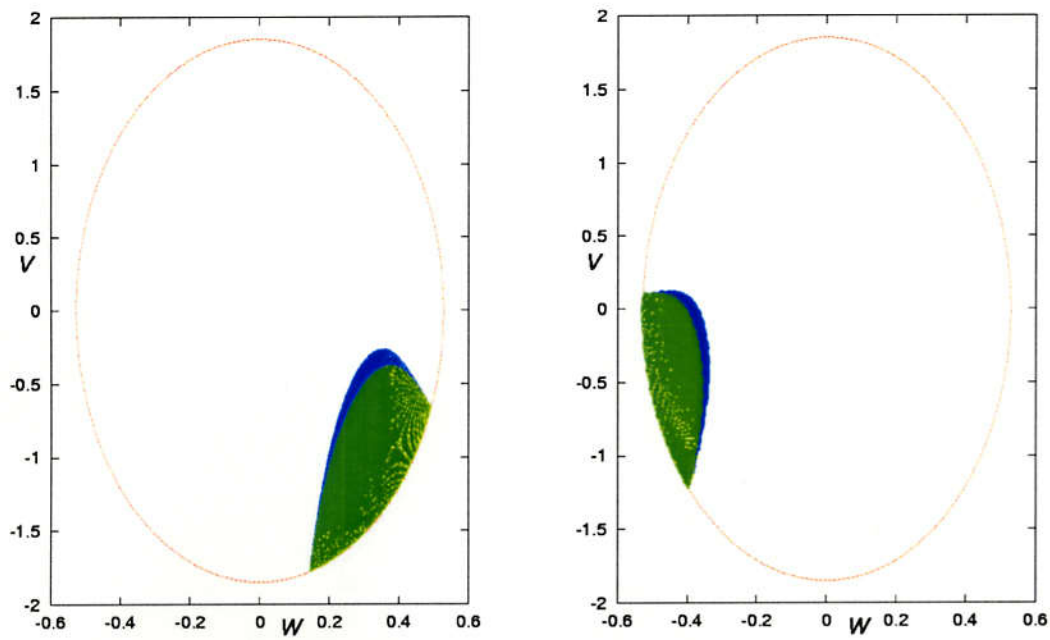

FIG.4.28: Regions I_{11} and $T(I_{11})$

Region I_{11} is displayed in the left. The image $T(I_{11})$ is displayed in the right. $T(I_{11})$ is mapped onto I_4.

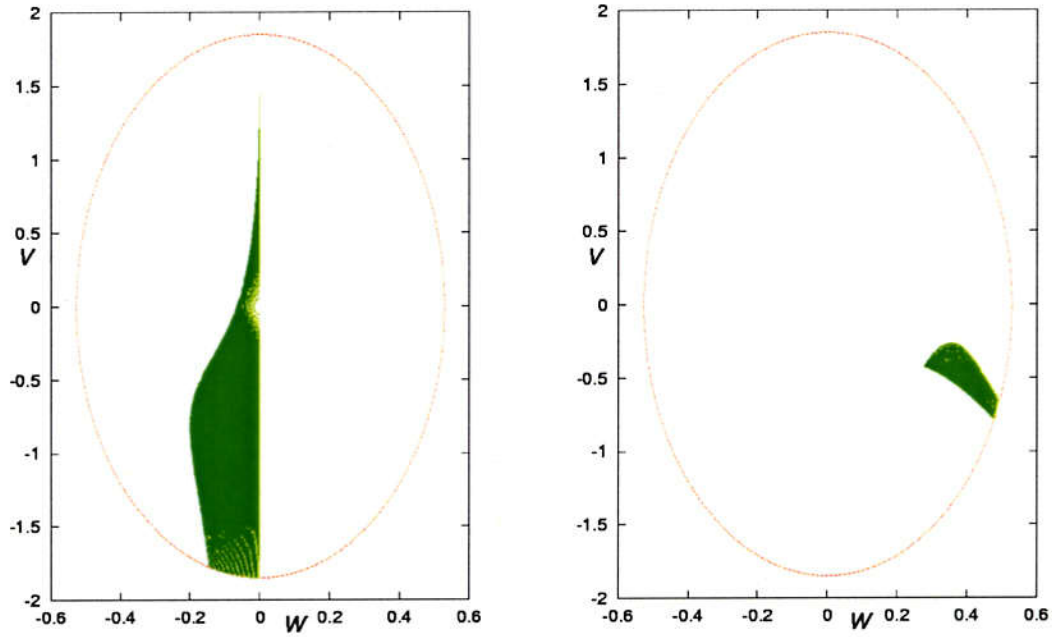

FIG.4.29: Regions I_6 and $T(I_6)$

Region I_6 is displayed in the left. The image $T(I_6)$ is displayed in the right. $T(I_6)$ is mapped onto I_{11}.

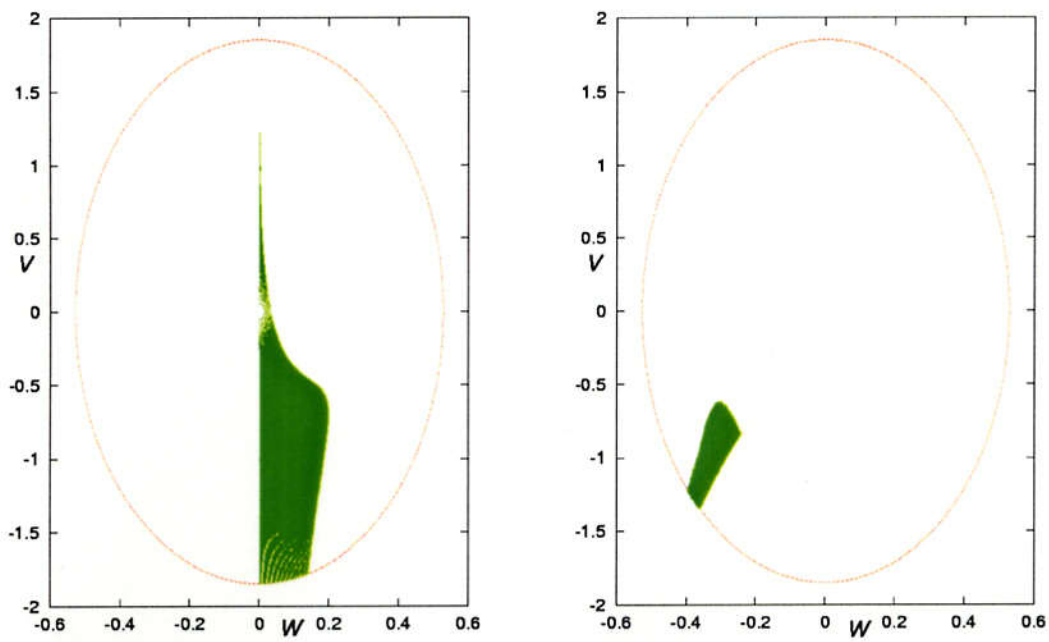

FIG.4.30: Regions I_{12} and $T(I_{12})$

Region I_{12} is displayed in the left. The image $T(I_{12})$ is displayed in the right. $T(I_{12})$ is mapped onto I_5.

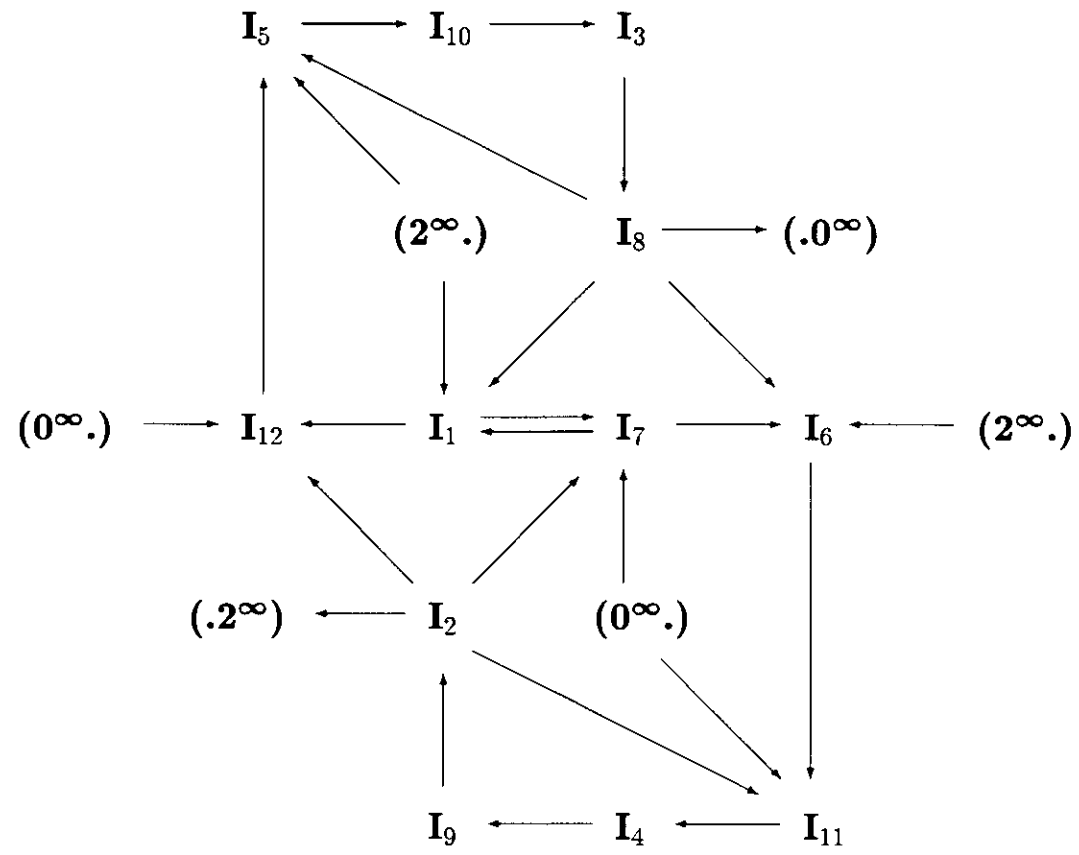

FIG.4.31: Transition Diagram

From Figs.4.19-30, we construct the transition diagram in the form of directed graph in Fig.4.31. Arrows in the graph denote the mapping. An arrow from I_i to I_j means that I_i is mapped into I_j. If we find a closed loop of one-directed arrows $I_i \rightarrow$, $I_{i+1} \rightarrow, \cdots \rightarrow, I_{i+k}$, then we have a possible period k.

The other way of finding a possible period is a transition matrix which is a matrix $A = (a_{ij})$ such that $a_{ij} = 1$ if $T(I_i) \cap I_j$ is nonempty and $a_{ij} = 0$ otherwise. In our case, the transiotion matrix is

$$A = \begin{bmatrix} O & B \\ B & O \end{bmatrix}, \tag{4.3.1}$$

where

$$B = \begin{bmatrix} 1 & 0 & 0 & 0 & 0 & 1 \\ 1 & 0 & 0 & 0 & 1 & 1 \\ 0 & 1 & 0 & 0 & 0 & 0 \\ 0 & 0 & 1 & 0 & 0 & 0 \\ 0 & 0 & 0 & 1 & 0 & 0 \\ 0 & 0 & 0 & 0 & 1 & 0 \end{bmatrix}. \tag{4.3.2}$$

Obviously we have

$$A^{2n} = \begin{bmatrix} B^{2n} & O \\ O & B^{2n} \end{bmatrix}, \qquad A^{2n+1} = \begin{bmatrix} O & B^{2n+1} \\ B^{2n+1} & O \end{bmatrix}. \tag{4.3.3}$$

These mean that possible period of arbitrary periodic points is some even number.

$$B^4 = \begin{bmatrix} 1 & 0 & 1 & 1 & 1 & 1 \\ 1 & 1 & 1 & 1 & 1 & 1 \\ 1 & 0 & 1 & 1 & 1 & 1 \\ 1 & 0 & 0 & 1 & 1 & 1 \\ 1 & 0 & 0 & 0 & 1 & 1 \\ 0 & 1 & 0 & 0 & 0 & 0 \end{bmatrix}, \quad B^5 = \begin{bmatrix} 1 & 1 & 1 & 1 & 1 & 1 \\ 2 & 1 & 1 & 1 & 2 & 2 \\ 1 & 1 & 1 & 1 & 1 & 1 \\ 1 & 0 & 1 & 1 & 1 & 1 \\ 1 & 0 & 0 & 1 & 1 & 1 \\ 1 & 0 & 0 & 0 & 1 & 1 \end{bmatrix}. \tag{4.3.4}$$

Then, we have the conclusion that possible period of the periodic points on Σ is 2, 4, or 10.

4.6 Stable Regions and Escape Regions

Again see Fig.4.13 where we plot QCC up to 31st depth. There are some large voids, to which we give letters "A" to "N", as summarized in Table 4.7.

Regions "A" and "H" correspond to the stable regions in Fig.4.34. Therefore, they are thoght to be invariant under the mapping T. Orbits starting from "A" immediately make a 2-2 binary collision (symbol 2), come back to "H", make a 1-2-1 binary collision(symbol 0), and return to "A" again. There is a stable periodic orbit, which is represented in the centers of "A" and "H" by "+" (see Fig.4.34), which we should call "Schubart orbit". We carry out further calculations to obtain longer words of

Region	Word	Comment
A	$[.(20)^{16}]$	bounded motion
B	$[.2^{32}]$	immediate escaper (without any other intersection with Σ)
C	$[.2^{\infty}]$	immediate escaper expected from the criterion
D	$[.20^{31}]$	delayed escaper(after some intersections with Σ)
E	$[.202^{30}]$	delayed escaper
F	$[.2020^{29}]$	delayed escaper
G	$[.20202^{28}]$	delayed escaper
H	$[.(02)^{16}]$	bounded motion
I	$[.0^{32}]$	immediate escaper
J	$[.0^{\infty}]$	immediate escaper expected from the criterion
K	$[.02^{31}]$	delayed escaper
L	$[.020^{30}]$	delayed escaper
M	$[.0202^{29}]$	delayed escaper
N	$[.02020^{28}]$	delayed escaper

Table 4.7: Symbol sequences in large voids in Fig.4.13.

symbols in regions "A" and "H", whose length is 128. Area shown in Fig.4.34 is a set of points whose words are $[.(20)^{64}]$ and $[.(02)^{64}]$. These are thought to include quasi-periodic points around the Schubart orbit. In fact, we have found some quasi-periodic points numerically, shown in Fig.4.34. There are appeared some long narrow antennae growing from the regions shown in Fig.4.34. They are thought to be stable manifolds of an unstable periodic points which has 16 representative points on Σ shown by "$\times$" in Fig.4.34.

Peripheral voids are all escape region where our escape criteria are numerically confirmed (Figs.4.32-33).

Orbits starting from the voids satisfy the criteria after some steps of numerical integrations. Regions "B", "C", "I" and "J" are immediate escape regions. Especially, our escape criteria are satisfied in "C" and "J". They go to positive infinity of

v along the unstable manifolds on C_0 associated with c^+ They are winding around two branches. Regions "D" and "K" are mapped on "I∪J" and "B∪C", respectively after a binary collision. Therefore, "D" and "K" are also escape regions. The other voids "E" etc are also escape regions, which are not immediate escaper, but delayed escaper. We summarize these relations in terms of T.

$$A = T(H), \quad H = T(A),$$

$$C \cup B = T(K) = T^2(E) = T^3(M) = T^4(G),$$

$$I \cup J = T(D) = T^2(L) = T^3(F) = T^4(N).$$

There are many small voids in bundles of QCCs faced on I∪J and B∪C (Fig.4.13). They are all escape regions as far as we examined.

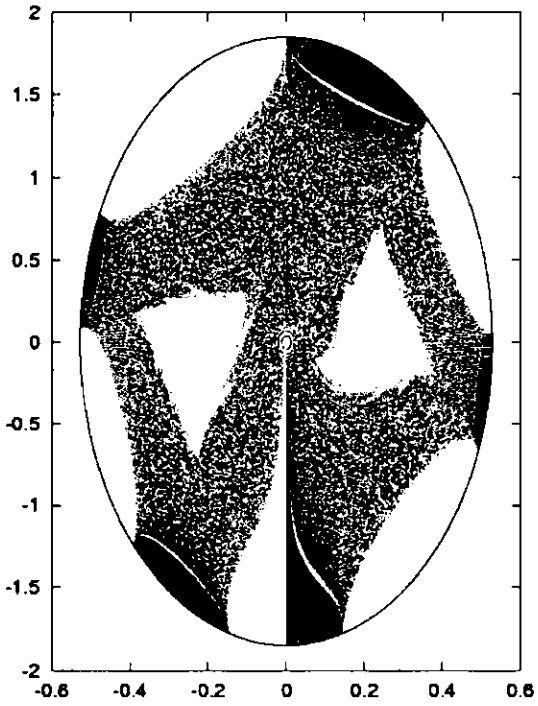

FIG.4.32: 1-2-1 escape region.

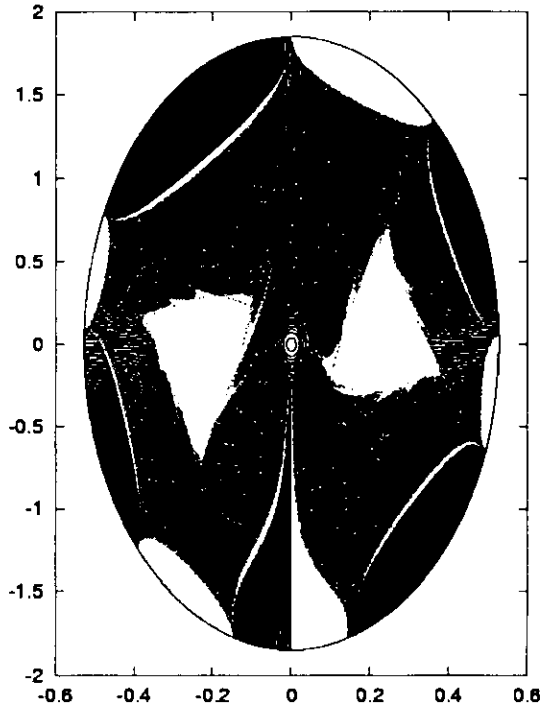

FIG.4.33: 2-2 escape region.

Using escape criteria obtained in theorems 3.5.1 and 3.5.2, we make a numerical survey of initial points on Σ leading to 1-2-1 escape or 2-2 escape. The results are shown in Figs.4.32-33. In Fig.4.32, we can see the points leading to 1-2-1 escape. In

Fig.4.33, we can see the points leading to 2-2 escape. In both Figs, escape points do not appear in the central two voids. This observation coincides with the search of stable region (Fig.4.34). The surrounding voids in Fig.4.32 are fulfilled by 2-2 escape points on Fig.4.33. On the contrary, the surrounding voids in Fig.4.33 are fulfilled by 1-2-1 escape points on Fig.4.32. Compare these figs with Fig.3.3 in the section 3.5 or Fig.4.13 in the section 4.3.

4.7 Families of Periodic Orbits

We numerically find some families of unstable periodic points. They are listed in Table 4.8. We give number of two digits to the families. First digit is the power of (02) or (20). Second digit is the number of 0 or 2 before (02) or (20). These are aligned perpendicularly to the stratified structure, and seem to accumulate to the boundary of escape regions.

Then, we have a conjecture about the existence of an infinite sequences of unstable periodic orbits and the existence of other families of unstable periodic orbits.

Stable manifolds associated to the unstable periodic points on Σ are observed to be extended along the stratified structure.

Order	Family 20	Family 22	Family 52	Family 50
1	$[0(20)^2]^\infty$	$[2(02)^2]^\infty$	$[2(02)^5]^\infty$	
2	$[00(20)^2]^\infty$	$[22(02)^2]^\infty$	$[22(02)^5]^\infty$	$[00(20)^222(02)^2]^\infty$
3		$[222(02)^2]^\infty$		$[000(20)^222(02)^2]^\infty$
4		$[2222(02)^2]^\infty$		

Table 4.8: Families of unstable periodic points

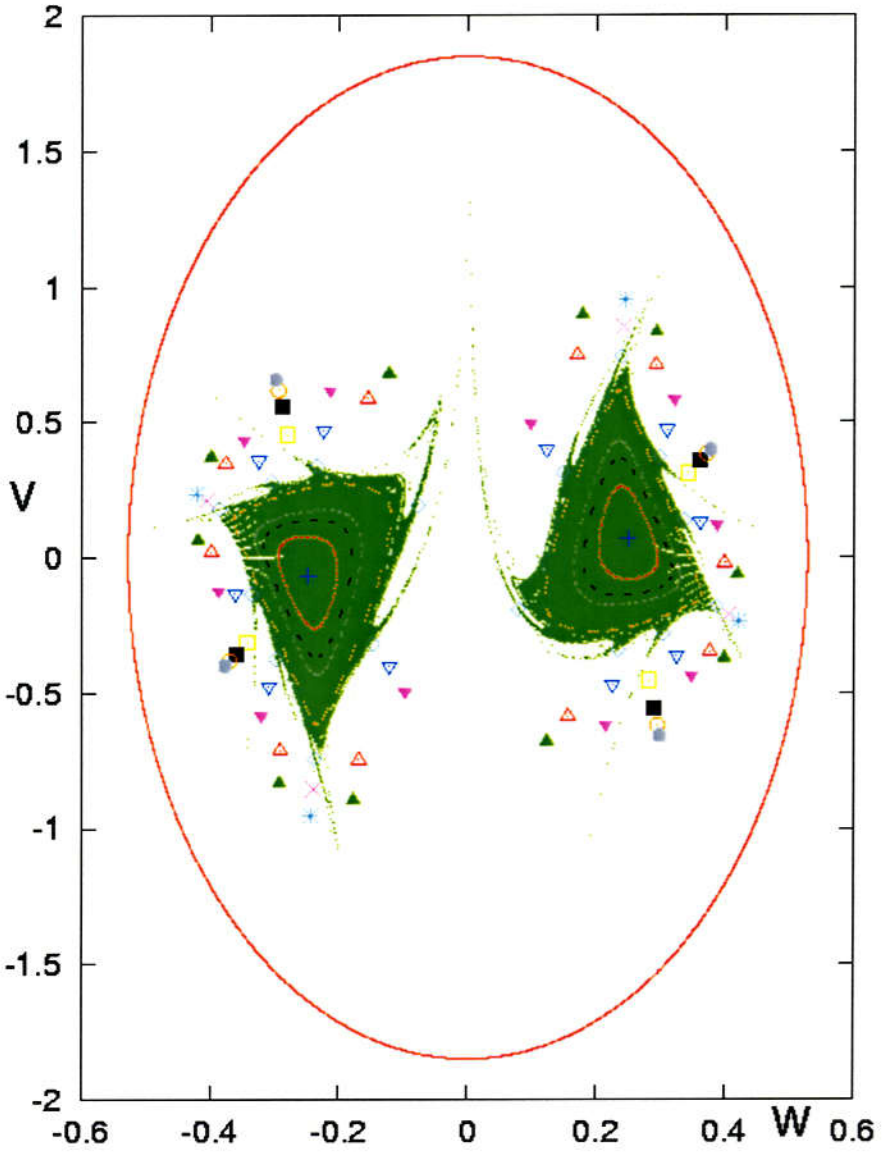

FIG.4.34: Unstable periodic points around the stable regions

Central green regions indicate the set of points whose word is $(20)^{128}$ or $(02)^{128}$. Symbol '+' in the center of the green regions indicate the Schubart type periodic points. Dotted curves and broken curves around '+' are thought to be quasi-periodic points. Othe symbols indicate unstable periodic points. The correspondence of symbols to periodic words is as follws. ⊡:$[2(02)^2]$, ■ :$[22(02)^2]$, ⊙ :$[222(02)^2]$, ● :$[2222(02)^2]$, × :$[0(20)^2]$, ✳ :$[00(20)^2]$, ▽:$[2(02)^5]$, ▼ :$[22(02)^5]$, △:$[00(20)^2 22(02)^2]$, ▲ :$[000(20)^2 22(02)^2]$, ◇:$[22(02)^8]$.

Chapter 5

Summary

The present study is the first systematic work on SC4BP. As far as concerned with SC4BP, analytical approaches to local structure near by quadruple collision or a numercal survey of surface of section ,which is not local were independently conducted in the previous studies. There were no research combining analytical tools and numerical tools largely. Through the both analytical and numerical approaches, we have the various features in the phase space of SC4BP. In this chapter, we summerize the present study.

5.1 Combination of the Typical Methods

We apply the method of *Symbolic Dynamics.* In SC4BP, almost all solutions experience binary collisions. Then, solutions for SC4BP are replaced by symbol sequences if binary collisions are replaced by symbols. This replacement emphasizes the qualitative differences among orbits while it ignores the quantitative differences. Therefore, this method is suitable for qualitative study where we pursue the geometrical structure of the phase space of SC4BP.

One of our analytical results *Surface of Section* is well-defined such as all solutions pass through the surface Σ once at least. Therefore, surface of section can be regarded as projection of the phase space where each orbit is regarded as fibre. Surface of section is a tool for investigation of global structure of the phase space. Thus,

our purpose is substituted by an exploration for distribution of symbol sequences over the surface of section Σ.

In order to execute such an exploration, we regularize binary collisions, and blow up quadruple collision. Regularization enables us to continue orbits beyond binary collision continuously. Blow-up technique enables us to analyze behavior of orbits in the vicinity of the quadruple collision. In addition, it is possible to connect the local phase structure around the quadruple collision and the global phase structure. Regularization and blow-up are achieved by defining new variables which are McGehee-llike. New variables are also applicable to numerical integrations. We embed the phase space into the 3-dimensional space using the new variables.

5.2 Analytical Results

First of our analytical results is the poperty with respect to the *Quadruple Collision Curves: QCC.* The set of initial points leading to quadruple collision forms 1-dimensional curves on Σ, which we call QCC. Outline of proof about the geometrical property is based on the fact that quadruple collision corresponds to two critical points on the McGehee's total collision manifold, one of which associates 2-dimensional stable manifold. In other word, QCC is intersection of the stable manifold and Σ.

Second is that Σ is a global surface of section as we mentioned above. Outline of its proof is based on the fact that each central force acting on m_2 or on the center of masses: m_1 and m_2 is montone with respect to ratio of distances. This monotoneity yeilds the other results: *Escape Criteria.* Outline of its proof is based on simple two-body considerations. There are two different escapes: *1-2-1 escape* and *2-2 escapes.* We display 3D-plot of the escape criteria with quadruple collision manifold. Also, we evaluate both escape criteria for these two types on Σ. Thus, one can comprehend the geometry of Σ and escape regions in the phase space. Moreover, escape criteria can be used in numerical calculations. They enable us to save time for calculations when the solution satisfies the criteria on the way of integration.

These two main results are based on the coordinates of McGehee. As many authors did, we define *Quadruple Collision Manifold: QCM*, which is one of invariant manifolds under the transformed flow. QCM is a two-dimensional manifold with 4 holes. The phase space of SC4BP is realized in the interior of the QCM. There are two critical points on QCM. Any solution begins from or ends up with quadruple collision is asymptotic to the critical points. Such solutions forms the so-called stable and unstable manifolds which are associated to the critical points. The stable and unstable manifolds are two dimensional in the real and physical pahse space of SC4BP, one dimensional curves on QCM which are winding themselves about QCM. The winding feature depends on mass-parameter. They are simple-connected manifolds, and devide the phase space of SC4BP into an infinity of subregions. Therefore, flows on QCM give a large influence to the global behavior as well as the local behavior of solutions near the quadruple collision. We show that the fictitious flow restricted on QCM is gradient-like with respect to v. This property influences the flow near the quadruple collision. We give an analytical expression of the homothetic solution which is uniquely determined for SC4BP. The homothetic solution connects two critical points on QCM.

If we summarize our analytical results and apply it to the surface of section Σ, then we can expect some stratified structure of Σ.

5.3 Numerical Results

We extensively conduct numerical calculation in the case of equal-masses and negative energy, which gives us a finer description of the structure in the surface of section Σ.

First, we otain QCCs as boundaries of subregions with different symbols. QCCs form several number of bunches whose end-points correspond to points where the invariant manifolds intersect the surface ofsection Σ. The surface of section Σ is divided into two subregions: *bunches* where QCCs exist densely, and *voids* where no QCC exists. Bunch regions were pointed out to be *chaotic area* in the previous

study. Our results show that the chaotic area has a stratified structure.

Application of *reversiblity* in Lemma 3.3.3 to the distribution of QCCs yields *un-realizable words*. Analytically, we show that [...0.0...], [...2.2...], [...1.2...] and [...2.1...] are un-reallizable words. Directly from numerical calculation, we obatin (...00.22...) etc. as un-realizable words, which are summarized in Table.[?]. We establish a rule which holds true among QCCs up to 13 of depth in order to give a conjecture that predicts all un-realizable words by assuming that the rule holds true for the deeper QCCs in general.

Second, the order of W_k perpendicular to W_k is not monotone while the order in collinear three-body problem is monotone. This observation is achievd by decimalization where symbol sequences are regarded as a ternary expansion of a certain real number. We plot the values versus the distance on Σ. The graph seems to be fractal, resembles to the famous devil's stair-case.

Third, we examine the voids in Σ. We calculate orbits starting from voids in Σ. Orbits starting from central voids stay in the voids for a long time, such that any orbits crosses two voids alternately. We calculate symbol words up to 128 of length in the central voids. Finer structure of the cental voids are observed. The results suggest the existence of some periodic orbits.

Orbits starting from other voids adjacent C_0 escape after a few crossing Σ at most. We obtain the initial points leading to escape using our escape criteria(Lemma 3.5.1 and 3.5.2). Observing the results, one can see such initial points almost everywhere in Σ except for the central voids.

Finally, we divide Σ into 12 subsets with based on QCCs, and construct the transition rule of mapping among the subsets, in order to obtain possible periodic words. We directly find some periodic words by numerical survey of Σ. They coincide with some of words expected from the transition rule.

Appendix A

The homothetic solution for SC4BP

Here we study the homothetic solution for SC4BP and the variational equations around it. We show the transversal intersection between the invariant manifold associated with the homothetic solution and the surface of section Σ.

The homothetic solution is a special solution for SC4BP in which the ratio of distance between particles is constant: $d\theta/ds \equiv 0$. Here, we use a set of equations (2.2.2) in order to obtain the homothetic solution. We require $d\theta/d\tau \equiv 0$, i.e., $u \equiv 0$ for the equations. This means to attain zeros of $dV(\theta)/d\theta$. As is easily seen, there is only one value of θ where $dV(\theta)/d\theta = 0$ because $d^2V(\theta)/d\theta^2 > 0$. We call the value of θ θ_c: $dV(\theta_c)/d\tau = 0$. The value θ_c is obtained from a root of the folowing equation.

$$T^7 - 2P^2T^5 - P^3(17P^2 + 8)T^4 + P^4T^3 + 2P^5(P^2 - 4)T^2 - P^9 = 0, \qquad (A1)$$

where $T \equiv \tan\theta_c$ and $P \equiv \tan\varphi$. Therefore, θ_c depends on mass parameter φ only. We display the relation in Fig.A.1 and Table.A.1. If $\varphi \to 0$ then $\theta_c \to 0$ and if $\varphi \to \pi/2$ then $\theta_c \to \pi/2$, otherwise $\theta_c > \varphi$. Using θ_c, we obtain the homothetic solution for negative energy level($h = -1$), i.e.,

$$(r_0, \theta_0, v_0, w_0) = (2\kappa^2\mathrm{sech}^2(s\lambda + \alpha), \theta_c, -2\kappa\tanh(s\lambda + \alpha), 0) \qquad (A2)$$

with $\kappa = \sqrt{V(\theta_c)/2}$, $\lambda = \sqrt{\cos\theta_c \sin(\theta_c - \varphi)/2}$ and a certain real number α. The solution approaches to the critical points c^- : $(0, \theta_c, -2\kappa, 0)$ as $s \to \infty$ and c^+ : $(0, \theta_c, 2\kappa, 0)$ as $s \to -\infty$.

Next, we study the variational equations for SC4BP around the homothetic solution. We define $(\delta_1, \delta_2, \delta_3, \delta_4)$ as variations of (r, θ, v, w), respectively. We express the homothetic solution by the suffix 0. The variational equations are obtained as follows.

$$\frac{d\delta_1}{ds} = \kappa_1(v_0\delta_1 + r_0\delta_3) + r_0 v_0 \kappa_2 \delta_2, \tag{A3.1}$$

$$\frac{d\delta_2}{ds} = \delta_4, \tag{A3.2}$$

$$\frac{d\delta_3}{ds} = -2\kappa_1\delta_1 - r_0\kappa_2\delta_2 - v_0\kappa_1\delta_3, \tag{A3.3}$$

$$\frac{d\delta_4}{ds} = -2\kappa_1\kappa_2(\delta_1 + v_0\delta_3) + \kappa_1\left(\frac{1}{\sqrt{W(\theta_c)}}\frac{d^2W(\theta_c)}{d\theta^2}\delta_2 - v_0\delta_4\right), \tag{A3.4}$$

where $\kappa_1 = \cos\theta_c \sin(\theta_c - \varphi)/\sqrt{W(\theta_c)}$ and $\kappa_2 = \cos(2\theta_c - \varphi)/\sqrt{W(\theta_c)}/2$. If we linearize the energy relation(2.2.8) around the homothetic solution, then we have

$$\delta_1 + v_0\delta_3 = 0. \tag{A4}$$

Applying (A4) to equations (A3)s provides the following equations.

$$\frac{d\delta_2}{ds} = \delta_4, \tag{A5.1}$$

$$\frac{d\delta_3}{ds} = -\frac{r_0\kappa_2}{2}\delta_2 + v_0\kappa_1\delta_3, \tag{A5.2}$$

$$\frac{d\delta_4}{ds} = \kappa_1\left(\frac{1}{\sqrt{W(\theta_c)}}\frac{d^2W(\theta_c)}{d\theta^2}\delta_2 - v_0\delta_4\right). \tag{A5.3}$$

In the limiting case of $s \to \mp\infty$, these equations determine the flow in the vicinity of the critical points $c^\pm$: $(0, \theta_c, \pm\sqrt{2V(\theta_c)}, 0)$, respectively. The equations $(A5)$s as $s \to \mp\infty$ become as follows.

$$\frac{d\delta_2}{ds} = \delta_4, \tag{A6.1}$$

$$\frac{d\delta_3}{ds} = \pm\delta_3\sqrt{2\cos\theta_c \sin(\theta_c - \varphi)}, \tag{A6.2}$$

$$\frac{d\delta_4}{ds} = \frac{\cos\theta_c \sin(\theta_c - \varphi)}{W(\theta_c)}\frac{d^2W(\theta_c)}{d\theta^2}\delta_2 \mp \sqrt{2\cos\theta_c \sin(\theta_c - \varphi)}\delta_4. \tag{A6.3}$$

All coefficients are constant. General solutions for (A6)s are characterized by eigenvalues of the coefficient matrix, i.e.,

$$\begin{pmatrix} 0 & 0 & 1 \\ 0 & \pm\sqrt{2\cos\theta_c \sin(\theta_c-\varphi)} & 0 \\ \frac{\cos\theta_c \sin(\theta_c-\varphi)}{W(\theta_c)} \frac{d^2W(\theta_c)}{d\theta^2} & 0 & \mp\sqrt{2\cos\theta_c \sin(\theta_c-\varphi)} \end{pmatrix}. \quad (A7)$$

The eigenvalues are

$$\lambda_1^{\pm} = \sqrt{\frac{\cos\theta_c \sin(\theta_c-\varphi)}{2}}\left(\mp 1 + \sqrt{1+\frac{2}{W(\theta_c)}\frac{d^2W(\theta_c)}{d\theta^2}}\right), \quad (A8.1)$$

$$\lambda_2^{\pm} = \pm\sqrt{2\cos\theta_c \sin(\theta_c-\varphi)}, \quad (A8.2)$$

$$\lambda_3^{\pm} = \sqrt{\frac{\cos\theta_c \sin(\theta_c-\varphi)}{2}}\left(\mp 1 - \sqrt{1+\frac{2}{W(\theta_c)}\frac{d^2W(\theta_c)}{d\theta^2}}\right). \quad (A8.3)$$

As is easily seen,

$$\lambda_1^{\pm} > 0, \quad \lambda_2^{+} > 0, \quad \lambda_2^{-} < 0, \quad \lambda_3^{\pm} < 0, \quad (A9)$$

Therefore, invariant manifolds associated with c^+: W_+^s is 1-dimensional, W_+^u is 2-dimensional. Invariant manifolds associated with c^-: W_-^s is 2-dimensional, W_-^u is 1-dimensional. The eigenvectors perpendicular to the homothetic solusion are

$$\begin{pmatrix} 1+\sqrt{1+\frac{2}{W(\theta_c)}\frac{d^2W(\theta_c)}{d\theta^2}} \\ 0 \\ \pm\frac{\sqrt{2\cos\theta\sin(\theta_c-\phi)}}{W(\theta_c)}\frac{d^2W(\theta_c)}{d\theta^2} \end{pmatrix} \quad \text{for} \quad \lambda_1^{\pm}, \quad (A10.1)$$

$$\begin{pmatrix} 1-\sqrt{1+\frac{2}{W(\theta_c)}\frac{d^2W(\theta_c)}{d\theta^2}} \\ 0 \\ \pm\frac{\sqrt{2\cos\theta\sin(\theta_c-\phi)}}{W(\theta_c)}\frac{d^2W(\theta_c)}{d\theta^2} \end{pmatrix} \quad \text{for} \quad \lambda_3^{\pm}, \quad (A10.2)$$

Both W_+^u and W_-^s intersect the surface of section Σ transversally in the vicinity of the critical points. In general, equations for δ_2 and δ_4 ((A5.1) and (A5.3)) are separable from (A5.2). They give normal components to the homothetic solution. From these eqations, we obtain the transversality mentioned above because $d\delta_2/ds \neq 0$ when $\delta_2 = 0$.

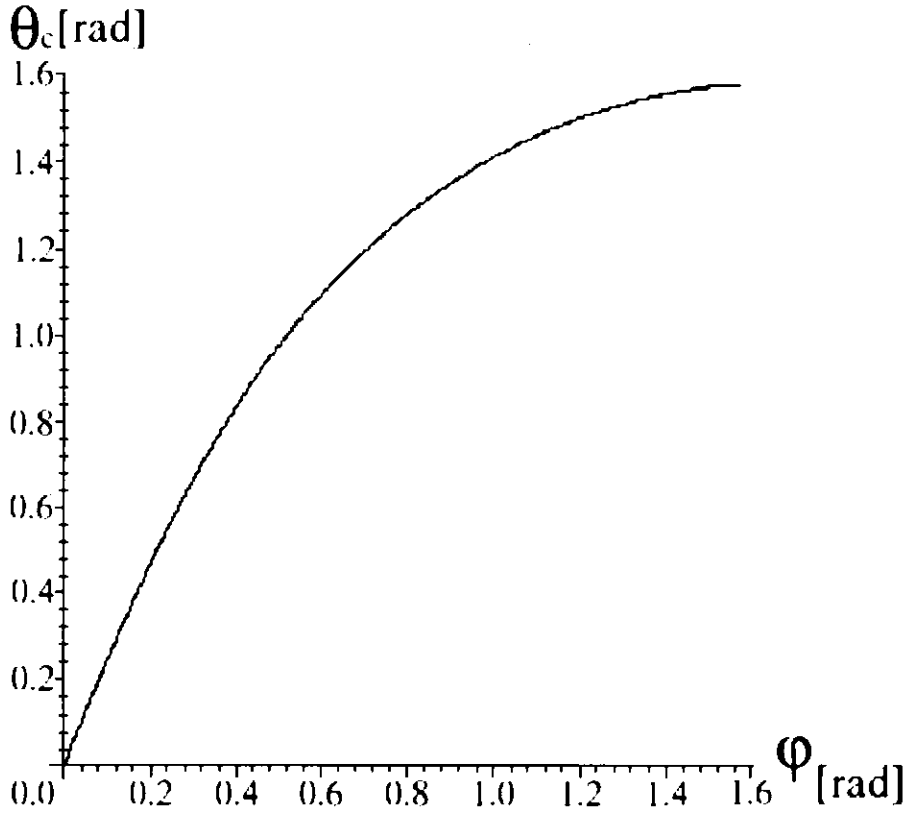

FIG. A.1: θ_c to φ curve

m_1	m_2	φ (rad)	θ_c (rad)
0.10	0.90	1.24905	1.51089
0.20	0.80	1.10715	1.45737
0.30	0.70	0.99116	1.40059
0.40	0.60	0.88608	1.33739
0.50	0.50	0.78540	1.26450
0.60	0.40	0.68472	1.17727
0.70	0.30	0.57964	1.06789
0.80	0.20	0.46365	0.92090
0.90	0.10	0.32175	0.69598

Table A.1: Values of φ and θ_c for masses

Bibliography

[1] Belbruno,E.: 1984, 'On simultaneous double collision in the collinear four-body problem', *J. Diff. Eq.*, **52**, 415-431.

[2] Dankowicz,H. and Holmes,P.: 1995, 'The existence of transverse homoclinic points in the Sitnikov Problem', *J. Diff. Eq.*, **116**, 468-483.

[3] Devaney,R.L.: 1980, 'Triple collision in the planar isosceles three-body problem', *Inventiones Mathematicae*, **60**, 249-267.

[4] Devaney,R.L.: 1981, 'Sigularities in classical mechanical systems', in A.Katok(ed.), 'Ergodic theory and dynamical systems I', *Prog. in Math.*, **10**, 211-333, Birkhauser, Basel.

[5] Devaney,R.L.: 1982, 'Blowing up singularities in classical mechanical systems', *Amer. Math. Mon.*, **89**, 535-552.

[6] Easton,R.: 1971, 'Some topology on the 3-body problem', *J. Diff. Eq.*, **12**, 361-384.

[7] Easton,R.: 1972, 'The topology of the regularized integral surface of the 3-body problem', *J. Diff. Eq.*, **12**, 361-384.

[8] Easton,R.: 1984, 'Parabolic orbits for the planar three-body problem', *J. Diff. Eq.*, **52**, 116-134.

[9] Fernández, J.D.: 1988, 'Transversal Ejection-collision orbits in Hll's problem for $c \gg 1$', *Cele. Mech.*, **44**, 299-307.

[10] Hietarinta,J. and Mikkola,S.: 1993, 'Chaos in the one-dimensional gravitational three-body problem', *CHAOS*, **3**, 183-203.

[11] Kaplan,S.R.: 1999, 'Symbolic dynamics of the collinear three-body problem', *Contemporary Mathematics*, **246**, 143-162.

[12] Lacomba,E.A.: 1981, 'Quadruple Collision in the Trapezoidal Four Body Problem', in 'Classical Mechanics and Dynamical Systems', 109-122, Marcel Dekker.

[13] Lacomba,E.A. and Losco,L.: 1981, 'Triple Collision in the Isosceles 3-Body Problem', *Bull. Am. Math. Soc.*, **3**, 710-714.

[14] Lacomba,E.A. and Pérez-Chavela,E.: 1992, 'A Compact Model For the Rhomboidal 4-Body Problem', *Celes. Mech. Dyn. Astr.*, **54**, 343-355.

[15] Lacomba,E.A. and Pérez-Chavela,E.: 1993, 'Motions Close to Escapes in the Rhomboidal Four Body Problem', *Celes. Mech. Dyn. Astr.*, **57**, 411-437.

[16] Lacomba,E.A. and Simoó,C.: 1992, 'Regularization of simultaneous binary collisions', *J. Diff. Eq.*, **98**, 241-259.

[17] Llibre,J.: 1982, 'On the restricted three-body problem when the mass parameter is small', *Celes. Mech.*, **28**, 83-105.

[18] Llibre,J. and Simó,C.: 1980, 'Oscillatory Solutions in the Planar Restricted Three-Body problem', *Math. Ann.*, **248**, 153-184.

[19] Marchal, C. and Saari, D.G.: 1976, 'On the final evolution of the n-body problem', *J. Diff. Eq.*, **20**, 150-186.

[20] Mather,J. and McGehee,R.: 1975, 'Solutions of the collinear four-body problem which become unbounded in finite time', *Dynamical systems theory and its applications*, 573-597, Lecture notes in physics, Springer-Verlag.

[21] McGehee,R.: 1974, 'Triple collision in the collinear three-body problem', *Inventiones Mathematicae*, **27**, 191-227.

[22] McGehee,R.: 1975, 'Triple collision in Newtonian gravitational systems', in J.Mather(ed.), *Lecture Notes in Physics*, **38**, 550-572, Springer-Verlag.

[23] McGehee,R.: 1978, 'Sigularities in classical mechanics', *Proc. Int. Cong. Math.*, 827-834, Helsinki.

[24] Meyer,K.R. and Wang,Q.D.:1995, 'The collinear three-body problem with negative energy', *J. Diff. Eq.*, **119**, 284-309.

[25] Mikkola,S.: 1983, 'Encounters of binaries — I. Equal energies', *M.N.R.A.S.*, **203**, 1107-1121.

[26] Mikkola,S.: 1984, 'Encounters of binaries — II. Unequal energies', *M.N.R.A.S.*, **204**, 115-126.

[27] Mikkola,S. and Hietarinta,J.: 1989, 'A Numerical investigation of the one-dimensional Newtonian three-body problem', *Celes. Mech.*, **46**, 1-18.

[28] Mikkola,S. and Hietarinta,J.: 1990, 'A Numerical investigation of the one-dimensional Newtonian three-body problem II', *Celes. Mech.*, **47**, 321-331.

[29] Mikkola,S. and Hietarinta,J.: 1991, 'A Numerical investigation of the one-dimensional Newtonian three-body problem III', *Celes. Mech.*, **51**, 379-394.

[30] Moeckel,R.: 1981, 'Orbits of the Three-Body Problem which pass infinitely close to Triple Collision', *Am. J. Math.*, **103**, 1323-1341.

[31] Moeckel,R.: 1983, 'Orbits near triple collision in the three-body problem', *Indiana Univ. Math. Journ.*, **32**, 221-240.

[32] Moeckel,R.: 1984, 'Heteroclinic Phenomena in the isosceles three-body problem', *SIAM J. Math. Anal.*, **15**, 857-876.

[33] Moeckel,R.: 1985, 'Relative Equilibria of the four-body problem', *Erg. Th. Dyn. Sys.*, **5**, 417-435.

[34] Moeckel,R.: 1989, 'Chaotic dynamics near triple collision', *Arch. Rational Mech. Anal.*, **107**, 37-69.

[35] Roy,A.E. and Steves,B.A.: 1998, 'Some special restricted four-body problems — II. From Caledonia to Copenhagen', *Planet. Space Sci.*, **46**(11/12), 1475-1486.

[36] Saari, D.G.: 1984, 'Sigularities and collisions of Newtonian gravitaional systems', *Arch. Rational Mech. Anal.*, **49**, 311-320.

[37] Saari, D.G.: 1984, 'The manifold structure for collision and for hyperbolic-parabolic orbits in the n-body problem', *J. Diff. Eq.*, **55**, 300-329.

[38] Saari, D.G. and Diacu, F.N.: 1994, 'Superhyperbolic expansion, noncollision singularities and symmetry cofigurations', *Cele. Mech.*, **60**, 91-98.

[39] Saari,D.G. and Xia,Z.: 1988, 'The existence of oscillatory and superhyperbolic Motion in Newtonian Systems', *J. Diff. Eq.*, **82**, 342-355.

[40] Samarov,K.L.: 1977, 'Regularization of the isosceles three-body problem for a non-zero area vector', *Soviet Math. Dokl.*, **18**, 245-249.

[41] Samarov,K.L.: 1977, 'Regularization of the isosceles three-body problem with zero area vector', *Soviet Math. Dokl.*, **18**, 558-562.

[42] Schubart,J.: 1956, *Astron. Nachr.*, **283**, 17.

[43] Sekiguchi,M. and Tanikawaa,K.: 1991, 'Orbits asymptotic to the outermost KAM in the restricted three-body problem',the proceedings of NATO ASI entitled 'Predictablity, Stability and Chaos in N-Body Dynamics', eds. A.E.Roy, 493-497, Prenum Press.

[44] Sekiguchi,M. and Tanikawa,K.: 2000, 'On Escape Orbits in the Symmetric Collinear Four-Body Problem', *Proceedings of the 32nd Symposium on Celestial Mechanics, Kanagawa, Japan, 15-17 Mar. 2000*, 311-315.

[45] Siegel,C.L. and Moser,J.K.: 1971, 'Lectures on Celestial Mechanics', *Springer-Verlag.*

[46] Simó,C.: 1978, 'Masses for which triple collision is regularizable', *Celes. Mech.*, **21**, 25-36.

[47] Simó,C. and Lacomba,E.: 1982, 'Analysis of some degenerate quadruple collisions', *Celes. Mech.*, **28**, 49-62.

[48] Simó,C. and Lacomba,E.: 1992, 'Regularization of simaultaneous binary collisions in the n-body problem', *J. Diff. Eq.*, **98**, 241-259.

[49] Simó,C. and Martinez,R.: 1988, 'Qualitative study of the planar isosceles problem', *Celes. Mech.*, **41**, 179-251.

[50] Simó,C. and Susín,A.: 1991, 'Connections between invariant manifolds in the collision manifold of the planar-three-body problem', in T.Ratiu(ed.), *The geometry of Hamiltonian systems*, 497-518, MSRI series, Springer-Verlag.

[51] Sitnikov,K.A.: 1960, 'Existence of oscillatory motions for the three-body problem', *Dokl. Akad. Nauk. USSR*, **133**, 303-306.

[52] Steves,B.A. and Roy,A.E.: 1998, 'Some special restricted four-body problems — I. Modeling the Caledonian problem', *Planet. Space Sci.*, **46**(11/12), 1465-1474.

[53] Sundman,K.: 1909, 'Nouvelles recherches sur le probleme des trois corps', *Acta Math.*, **35**, No.9.

[54] Sundman,K.: 1912, 'Memoire sur le probleme des trois corps', *Acta Math.*, **36**, 105-179

[55] Sweatman,W.: 'The symmetrical one-dimensional Newtonian four-body problem: A numerical Investigation', *Celes. Mech. Dyn. Astr.*, to appear.

[56] Tanikawa,K. and Mikkola,S.: 2000, 'Triple collisions in the one-dimensional three-body problem', *Celes. Mech. Dyn. Astr.*, **76**, 23-34.

[57] Tanikawa,K. and Mikkola,S.: 2000, 'One-dimensional three-body problem via symbolic dynamics', *CHAOS*, **10**, 649-657.

[58] Tanikawa,K. and Mikkola,S.: 2000, 'Multiple collisions in the one-dimensional free-fall four-body problem', *Proceedings of the 32nd Symposium on Celestial Mechanics, Kanagawa, Japan, 15-17 Mar. 2000*, 297-310.

[59] Vidal,C.: 1999, 'The tetrahedral 4-body problem with rotation', *Celes. Mech. Dyn. Astr.*, **71**, 15-33.

[60] Waldvogel,J.: 1976, 'The three-body problem near triple collision', *Cele. Mech.*, **14**, 287-300.

[61] Waldvogel,J.: 1982, 'Symmetric and regularized coordinates on the plane triple collision manifold',

[62] Xia,Z.: 1992, 'Melnikov method and transversal homoclinic points in the restricted three-body problem', *J. Diff. Eq.*, **96**, 170-184.

[63] Xia,Z.: 1992, 'The existence of noncollision singularities in newtonian systems', *Ann. Math.*, **135**, 411-468.

[64] Xia,Z.: 1994, 'Arnold diffusion and oscillatory solutions in the three-body problem', *J. Diff. Eq.*, **110**, 289-321.

[65] Zare,K. and Chesley,S.: 1998, 'Order and chaos in the planar isoceles three-body problem', *CHAOS*, **8**, 475-494.